

Three-dimensional and free-edge hygrothermal stresses in general long sandwich plates

Isa Ahmadi*

*Advanced Materials and Computational Mechanics Lab, Department of Mechanical Engineering,
University of Zanjan, 45371-38791, Zanjan, Iran*

(Received April 22, 2017, Revised October 29, 2017, Accepted November 21, 2017)

Abstract. The hygrothermal stresses in sandwich plate with composite faces due to through the thickness gradient temperature and (or) moisture content are investigated. The layer-wise theory is employed for formulation of the problem. The formulation is derived for sandwich plate with general layer stacking, subjected to uniform and non-uniform temperature and moisture content through the thickness of the plate. The governing equations are solved for free edge conditions and 3D stresses are investigated. The out of plane stresses are obtained by equilibrium equations of elasticity and by the constitutive law and the results for especial case are compared with the predictions of a 3D finite element solution in order to study the accuracy of results. The three-dimensional stresses especially the free edge effect on the distribution of the stresses is studied in various sandwich plates and the effect of uniform and non-uniform thermal and hygroscopic loading is investigated.

Keywords: thermal loading; hygroscopic loading; sandwich plate; out of plane stresses; layer-wise theory

1. Introduction

The mechanical properties of advanced laminated composite materials have some advantageous with respect to conventional engineering materials such as metals. The main advantages of composite material are high strength to weight and high modulus to weight ratio of these materials which make them favorite materials for use in weight sensitive structures with high strength and high stiffness and low weight. So the application of laminated composite and sandwich structures with laminated faces increased in aerospace, automotive, civil and sport industries which weigh is very important parameter. Composite and sandwich structures usually work in non-isothermal or humid environment and so hygrothermal loading must be studied for these structures. The coefficient of thermal expansion and moisture expansion of core and faces in the sandwich structures are different and face and core tend to expand (contract) differently due to change in temperature and moisture content. So, thermal and hygroscopic stresses grow in composite and sandwich structures. Furthermore, the out of plane stresses arise at a thin layer at the vicinity of edges, and usually complex 3D stress state occurs near the edges of these structures which is called boundary layer and may results in delamination and transverse cracking at the interface of plies such as core-face interface especially near the free edges.

The 2D theories of composite plate and shells are not able to predict accurately the 3D stresses in boundary layer and many technical methods are employed by the

researchers to investigate the transverse stresses and 3D stress state analytically and numerically at vicinity of edges in composite and sandwich structures. Kant and Swaminathan (2000) and Mittelstedt and Becker (2004) reviewed various techniques which are employed by the researchers to evaluate the interlaminar and transverse stresses in composite plates and shells.

Hayashi (1967) and Puppo and Evensen (1970) presented analytical study to predict the interlaminar shear stresses in the laminated composite plates. Pagano (1974) studied the edge-effect and interlaminar problem of composite laminates due to thermal loading. Wang and Choi (1982) present an approximate elasticity solution to determine the boundary-layer stresses due to hygroscopic loading. Wang and Crossman (1977) used a finite element method to predict the free-edge stresses in symmetric balanced laminates under a uniform thermal load. Herakovich (1976) studied the free edge effects in composite laminates subjected to thermal loading using the finite element method. Farley and Herakovich (1978) employed FEM to study the interlaminar stresses for mechanical, uniform hygrothermal, and gradient moisture loading conditions. In their work, the non-uniform, two-dimensional hygroscopic gradients are obtained from a finite-difference solution of the diffusion equation and the numerical results show that hygroscopic-induced stresses can be larger than those of resulting from mechanical and thermal loading. Wang and Chou (1989) studied the transient three-dimensional thermal stresses in elastic, angle-ply laminated composites which are subjected to changes in the thermal boundary conditions.

In order to calculate the interlaminar shear stresses, Lu and Liu (1992) present a laminate theory which satisfies the interlaminar shear stress and the transverse shear deformation continuity. They verified the work by Pagano's

*Corresponding author, Associate Professor
E-mail: i_ahmadi@znu.ac.ir

elasticity analysis. Morton and Webber (1993a) present an analytical method using the principle of minimum complementary energy to predict the free-edge stresses due to thermal loading. Then they employed a quadratic interlaminar stress criterion to predict the interlaminar failure at the free edges of laminated composite plate which is subjected to mechanical and thermal loads (Morton and Webber, 1993b). Yin (1994) used Lekhnitskii's stress functions and principle of complementary virtual work and presented an approximate method for analysis of free-edge stresses in composite laminates under thermal and mechanical loads. Kim and Atluri (1995) studied the edge stress in the composite laminates which is subjected to combine thermal and mechanical loading conditions using the stress based variational method. Davi and Milazzo (1997) employed the boundary element method to study the free edge stresses and its singularity in composite laminates under uniform axial extension. Lee and Kim (1997) studied the residual thermal stresses at the interface corner between the fiber and the matrix of a two-dimensional unidirectional laminate due to cooling from cure temperature down to room temperature by boundary element method.

Cho and Kim (2000) used an iterative approach to study the free edge stresses in composite laminates which are subjected to combination of mechanical and thermal load. Their results satisfied the traction free conditions at the top and bottom surfaces. Pantano and Averill (2000) used a plate theory and a 3D finite element based on the first-order zig-zag approximation for thermal stress analysis of composite and sandwich laminates. Patel *et al.* (2002) used a higher order theory to study the response of the laminated composite plates under hygrothermal loading. Vaddadi *et al.* (2003) studied the transient hygrothermal stresses in the fiber-reinforced composites by a novel heterogeneous characterization approach. Tahani and Nosier (2003) studied the free edge effect in cross-ply composite plate subjected to uniform extension and uniform thermal loading using layerwise method. Matsunaga (2004) presented a two-dimensional global higher-order deformation to study the interlaminar stresses and displacements in cross-ply composite and sandwich plates subjected to thermal loadings. The numerical results are compared with those of the published three-dimensional layerwise theory. Naidu and Sinha (2005) investigated the large deflection bending behavior of composite cylindrical panels in hygrothermal environments using a finite element formulation.

Duong Nguyen and Hung Nguyen (2007) applied the metis element method to study the interlaminar stresses and delamination of composite laminates under extension and bending. Zhu *et al.* (2007) studied the dynamic interlaminar stress in laminated plates in free vibration and thermal load based on the thermo-elasto-dynamic differential equations. An analytical approach was proposed by Benkhedda *et al.* (2008) to calculate the hygrothermal stresses in laminated composite plates in which the change of mechanical characteristics because of moisture content and temperature change is considered. They considered the distribution of the transient in-plane stresses through the laminate thickness, whereas the transverse stresses were not taken into account in their work.

Lo *et al.* (2010) proposed a four-node quadrilateral plate

element based on the global-local higher order theory (GLHOT) to study the response of laminated composite plates due to a variation in temperature and moisture concentrations. Ahmadi and Aghdam (2010 a, b) present a micromechanical model to study the mechanical and thermal stresses in composite materials using a meshless method. Kim *et al.* (2010) presented an analysis based on the stress function to provide an approximation method of 3D stresses near the free edge of bonded composite patches. Brischetto (2012) analyzed the effects of hygrothermal loading in the bending of multilayered composite plates. Zenkour (2012) studied a FGM plate under a transverse uniform static loading which is exposed to hygrothermal conditions. The elastic coefficients, thermal coefficient and moisture expansion coefficient of the plate are assumed to be exponentially graded in the thickness direction.

Nath and Kapuria (2013) presented a coupled global-local theory (GLT) with 11 displacement unknowns and a zigzag-local theory (ZLT) with nine unknowns for hybrid plate to predict the transverse shear stresses under electromechanical loading. Brischetto (2013) proposed a refined two-dimensional model in the framework of the Carrera's unified formulation by considering both equivalent single layer and layerwise multilayer description for hygrothermoelastic analysis of composite and sandwich shells. Goodsell *et al.* (2013) developed the earlier works for modeling of finite width laminate to consider the anticlastic bending. They combined bending and torsion moments to yield a deformation state without twisting curvature and with transverse curvature due only to the laminate Poisson effect which is termed anticlastic bending.

Zenkour *et al.* (2014) investigated the effect of hygrothermal conditions on the antisymmetric cross-ply laminates using a unified shear deformation plate theory. The presented plate theory enables the trial and testing of different through-the-thickness transverse shear-deformation distributions. Hang and Kim (2015) applied an iterative method to analyze the free edge interlaminar stresses of piezo-bonded composite laminates in which electric field resulting in pure extension of the whole structure. Murugesan and Rajamohan (2015, 2016) investigated the combined effects of thermal and mechanical loadings on the distribution of interlaminar shear stresses in composite laminated composite beams and plates using the commercially available software package MSC NASTRAN/PATRAN. The validity of the finite element analysis is demonstrated by comparing the interlaminar shear stresses evaluated using the experimental measurement. Ahmadi (2016) studied edge stresses in thick composite panel subjected to pure extension using layerwise formulation. Goodshell and Pipes (2016) present a family of analytic solution for free edge interlaminar stress analysis in angle-ply composite laminates subjected to uniaxial extension, uniform temperature change and anticlastic bending. Padhi and Pandit (2016) used the higher-order zig-zag theory and studied the behavior of sandwich laminates subjected to thermal loading. Ahmadi (2016) and Ahmadi and Najafi (2016) studied the interlaminar stresses in closed sandwich and composite cylinder subjected to axi-symmetric hygrothermal and mechanical loading conditions. Recently, Boukert *et al.*

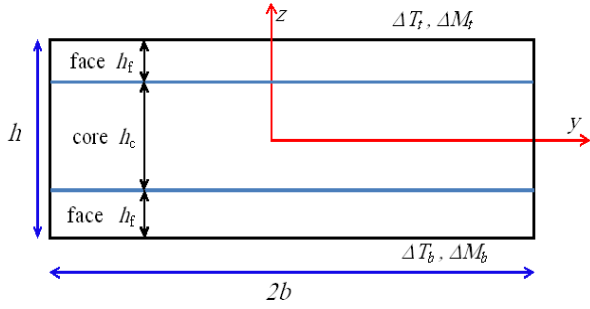


Fig. 1 Cross section of the sandwich plate, dimensions, yz coordinate system and loading

(2017) employed the higher order theory to predict the hygro-thermo-mechanical properties of thick composite plates. Ahmadi (2017) studied the interlaminar stresses in long sandwich plate using a Galerkin layerwise formulation. Singh and Chakrabarti (2017) developed a C^0 FE model based on higher order zigzag theory for hygrothermal analysis of laminated composite plates which satisfies the inter-laminar shear stress continuity at the interfaces.

The aim of this study is to predict accurately the distribution of three-dimensional and edge hygrothermal stresses in the core, faces and at the core/face interfaces of sandwich plate. A three-dimensional formulation is presented in order to obtain an accurate solution to study the global and local response of general thick sandwich plate which is subjected to uniform and through the thickness distributed hygrothermal loading conditions. The governing equations of plate are obtained employing the principle of minimum total potential energy and solved for free edge conditions. The accuracy of the results is examined by comparison of the results of present study by prediction of finite element formulation. The thermal and hygroscopic stresses distribution at the interfaces of layers and in the boundary layer region of the sandwich plate is studied for various layer stacking and uniform and non-uniform thermal and hygroscopic loading. The distribution of the stresses for uniform and through the thickness distributed hygrothermal loading is compared. To the knowledge of the author, this is the first time that such formulation with analytical solution is presented for sandwich plate which is subjected to hygrothermal loading condition.

2. Mathematical modeling

A laminated composite or sandwich plate with free edges is considered. The plate is subjected to temperature change and (or) moisture content change in which the temperature and moisture content change is uniform in the length and width of the plate and may have gradient in the plate thickness. The length, width and thickness of the plate are taken as $2L$, $2b$ and h , respectively. The x , y and z coordinates are the length, width and thickness coordinates of the plate, respectively, and the coordinate system is located in the plate center, and the edges of the plate at $y=\pm b$ and $x=\pm L$ are free. The yz cross-section of the sandwich plate is shown in Fig. 1. The plate is long in the x -

direction and the temperature change and moisture content change are uniform in the length and width of the plate, so it can be supposed that the strains in the plate do not depend on the length coordinate, unless near the edges at $x=\pm L$.

Considering that strains in the plate are independent of the x -coordinate, and u_1 , u_2 and u_3 are the displacements in the x , y and z direction, it can be shown that the displacement field of the plate can be expressed as (Lekhnitskii 1981)

$$\begin{aligned} u_1(x, y, z) &= C_5 xz + C_6 x + u(y, z) \\ u_2(x, y, z) &= -C_3 xz + v(y, z) \\ u_3(x, y, z) &= -\frac{1}{2} C_5 x^2 + C_3 xy + w(y, z) \end{aligned} \quad (1)$$

The rigid body motion and rigid body rotation of the plate are ignored in (1), and C_3 , C_5 and C_6 represent the global twisting, bending (curvature) and extension of the plate due to thermal and hygroscopic loading conditions.

The layerwise theory (LWT) is employed for discretization of the problem to ordinary differential equations. Layerwise theory assumes that the plate is made of N (arbitrary number) imagined layers which are so-called numerical layers and the interface of numerical layers are called numerical surface. The displacement functions $u(y,z)$, $v(y,z)$ and $w(y,z)$ (see Eq.(1)) on the i^{th} numerical surface are shown by $U_i(y)$, $V_i(y)$, and $W_i(y)$, $i=1,2,\dots,N+1$, respectively. In the layer-wise theory (LWT), the displacement functions $u(y,z)$, $v(y,z)$ and $w(y,z)$ are interpolated through the thickness of the plate based on $U_i(y)$, $V_i(y)$, and $W_i(y)$ and by employing the interpolations function $\Phi_k(z)$ as

$$\begin{aligned} u(y, z) &= U_k(y) \Phi_k(z) \\ v(y, z) &= V_k(y) \Phi_k(z) \quad k = 1, \dots, N+1 \\ w(y, z) &= W_k(y) \Phi_k(z) \end{aligned} \quad (2)$$

The interpolation function $\Phi_k(z)$ which is used in (2) is defined in the Appendix, and dummy index means summation from 1 to $N+1$, where $N+1$ is the number of numerical surfaces. By substituting (2) into displacement field in (1), and using the strain-displacement relation, the infinitesimal strains components can be obtained as

$$\begin{aligned} \varepsilon_x &= C_6 + C_5 z, & \varepsilon_{yz} &= V_k \Phi'_k + W'_k \Phi_k, \\ \varepsilon_y &= V'_k \Phi_k, & \varepsilon_{xz} &= U_k \Phi'_k + C_3 y, \\ \varepsilon_z &= W_k \Phi'_k, & \varepsilon_{xy} &= U'_k \Phi_k - C_3 z, \end{aligned} \quad (3)$$

Φ'_k is derivation of $\Phi_k(z)$ with respect to z and U'_k , V'_k and W'_k are derivation of $U_k(y)$, $V_k(y)$, and $W_k(y)$ with respect to y -coordinate. For a plate that is in the static equilibrium condition and there are no external forces on it, the principle of minimum total potential energy can be written as

$$\delta U = \int_{-L}^L \int_{-b}^b \int_{-h}^h \sigma_{ij} \delta \varepsilon_{ij} = 0 \quad (4)$$

in and the boundary conditions of the plate are obtained. The governing equations of the plate are obtained by

substituting the strain components from (3) into (4) as

$$\begin{aligned} M_{xy,y}^k - Q_x^k &= 0, \\ M_{y,y}^k - Q_y^k &= 0, \quad k = 1, 2, \dots, N + 1 \\ R_{y,y}^k - N_z^k &= 0, \end{aligned} \tag{5}$$

$$\begin{aligned} \int_{-b}^b \int_{-h/2}^{h/2} \sigma_x dz dy &= 0 \\ \int_{-b}^b \int_{-h/2}^{h/2} \sigma_x z dz dy &= 0 \\ \int_{-b}^b \int_{-h/2}^{h/2} (\sigma_{xz} y - \sigma_{xy} z) dz dy &= 0 \end{aligned} \tag{6}$$

in which $M_{xy}^k, M_y^k, R_y^k, Q_x^k, Q_y^k,$ and N_z^k in (5) are defined as

$$\begin{aligned} (M_{xy}^k, Q_x^k) &= \int_{-h/2}^{h/2} (\sigma_{xy} \Phi_k, \sigma_{xz} \Phi_k') dz \\ (M_y^k, Q_y^k) &= \int_{-h/2}^{h/2} (\sigma_y \Phi_k, \sigma_{yz} \Phi_k') dz, \quad k = 1, \dots, N + 1 \\ (R_y^k, N_z^k) &= \int_{-h/2}^{h/2} (\sigma_{yz} \Phi_k, \sigma_z \Phi_k') dz \end{aligned} \tag{7}$$

and are called stress resultants in LWT. Furthermore, the boundary conditions of the plate for free edge at $y=\pm b$ are obtained from the principle of minimum total potential energy (4) as

$$\begin{aligned} M_y^k (y = \pm b) &= 0, \\ R_y^k (y = \pm b) &= 0, \quad k = 1, 2, \dots, N + 1 \\ M_{xy}^k (y = \pm b) &= 0, \end{aligned} \tag{8}$$

The temperature and moisture content changes are uniform in the length and width of the plate and have gradient in the plate thickness. The temperature change is shown by $T(z)$ and moisture content change is shown by $M(z)$. The constitutive law of the k^{th} numerical layer in the plate which is subjected to temperature change and moisture content change can be written as

$$\begin{aligned} \begin{Bmatrix} \sigma_x \\ \sigma_y \\ \sigma_z \\ \sigma_{yz} \\ \sigma_{xz} \\ \sigma_{xy} \end{Bmatrix}^{(k)} &= \begin{bmatrix} \bar{C}_{11} & \bar{C}_{12} & \bar{C}_{13} & 0 & 0 & \bar{C}_{16} \\ \bar{C}_{12} & \bar{C}_{22} & \bar{C}_{23} & 0 & 0 & \bar{C}_{26} \\ \bar{C}_{13} & \bar{C}_{23} & \bar{C}_{33} & 0 & 0 & \bar{C}_{36} \\ 0 & 0 & 0 & \bar{C}_{44} & \bar{C}_{45} & 0 \\ 0 & 0 & 0 & \bar{C}_{45} & \bar{C}_{55} & 0 \\ \bar{C}_{16} & \bar{C}_{26} & \bar{C}_{36} & 0 & 0 & \bar{C}_{66} \end{bmatrix} \times \\ \begin{Bmatrix} \varepsilon_x - \alpha_x T(z) - \beta_x M(z) \\ \varepsilon_y - \alpha_y T(z) - \beta_y M(z) \\ \varepsilon_z - \alpha_z T(z) - \beta_z M(z) \\ \gamma_{yz} \\ \gamma_{xz} \\ \gamma_{xy} - \alpha_{xy} T(z) - \beta_{xy} M(z) \end{Bmatrix}^{(k)} \end{aligned} \tag{9}$$

in which $\bar{C}_{pq}^{(k)}$ are the stiffness matrix of k^{th} numerical layer, and for example, $\alpha_x^{(k)}$ and $\beta_x^{(k)}$ indicate the coefficient of thermal expansion and moisture expansion of k^{th} numerical layer in the x -direction, respectively. The distribution of temperature and moisture content change in the plate thickness can be discretized by the LW discretization approach as

$$\begin{aligned} T(z) &= T_k \Phi_k(z) \\ M(z) &= M_k \Phi_k(z) \end{aligned} \tag{10}$$

in which T_k and M_k are the temperature and moisture content change of the k^{th} numerical surface, respectively, and $\Phi_k(z)$ is the linear Lagrangian interpolation function which is defined in the Appendix. It must be noted that T_k and M_k are the known constants through the problem solution.

By substituting the strains from (3) and temperature and moisture change from (10) into (9), and substituting the subsequent results into (7), the stress resultants are obtained in terms of displacement and hygrothermal loading as

$$\begin{aligned} M_{xy}^k &= B_{16}^k C_6 + \tilde{B}_{16}^k C_5 - \tilde{B}_{66}^k C_3 + D_{26}^{kj} V_j' + B_{36}^{kj} W_j \\ &\quad + D_{66}^{kj} U_j' - D_{6T}^{kj} T_j - D_{6M}^{kj} M_j \\ M_y^k &= B_{12}^k C_6 + \tilde{B}_{12}^k C_5 - \tilde{B}_{26}^k C_3 + D_{22}^{kj} V_j' + B_{23}^{kj} W_j \\ &\quad + D_{26}^{kj} U_j' - D_{2T}^{kj} T_j - D_{2M}^{kj} M_j \\ N_z^k &= A_{13}^k C_6 + \tilde{A}_{13}^k C_5 - \tilde{A}_{36}^k C_3 + B_{23}^{jk} V_j' + A_{33}^{kj} W_j \\ &\quad + B_{36}^{jk} U_j' - B_{3T}^{jk} T_j - B_{3M}^{jk} M_j \\ Q_x^k &= A_{45}^{kj} V_j + B_{45}^{jk} W_j' + A_{55}^{kj} U_j + A_{55}^k C_3 y \\ Q_y^k &= A_{44}^{kj} V_j + B_{44}^{jk} W_j' + A_{45}^{kj} U_j + A_{45}^k C_3 y \\ R_y^k &= B_{44}^{kj} V_j + D_{44}^{kj} W_j' + B_{45}^{kj} U_j + B_{45}^k C_3 y \end{aligned} \tag{11}$$

where the mechanical rigidity matrixes which are appeared in (11) are defined as

$$\begin{aligned} A_{pq}^{kj} &= \sum_{i=1}^N \int_{z_i}^{z_{i+1}} \bar{C}_{pq}^{(i)} \Phi_k' \Phi_j' dz \\ B_{pq}^{kj} &= \sum_{i=1}^N \int_{z_i}^{z_{i+1}} \bar{C}_{pq}^{(i)} \Phi_k \Phi_j' dz \\ D_{pq}^{kj} &= \sum_{i=1}^N \int_{z_i}^{z_{i+1}} \bar{C}_{pq}^{(i)} \Phi_k \Phi_j dz \end{aligned} \tag{12}$$

$$\begin{aligned} (A_{pq}^k, B_{pq}^k) &= \sum_{i=1}^N \int_{z_i}^{z_{i+1}} \bar{C}_{pq}^{(i)} (\Phi_k', \Phi_k) dz \\ (\tilde{A}_{pq}^k, \tilde{B}_{pq}^k) &= \sum_{i=1}^N \int_{z_i}^{z_{i+1}} \bar{C}_{pq}^{(i)} (\Phi_k' z, \Phi_k z) dz \end{aligned} \tag{13}$$

and the matrixes of thermal and hygroscopic effect are defined as

$$\begin{aligned} (B_{pT}^{kj}, D_{pT}^{kj}) &= \sum_{i=1}^N \int_{z_i}^{z_{i+1}} \lambda_p^{(i)} (\Phi_k \Phi_j', \Phi_k \Phi_j) dz \\ (B_{pM}^{kj}, D_{pM}^{kj}) &= \sum_{i=1}^N \int_{z_i}^{z_{i+1}} \mu_p^{(i)} (\Phi_k \Phi_j', \Phi_k \Phi_j) dz \end{aligned} \quad (14)$$

where $\{\lambda\}$ and $\{\mu\}$ are defined in (A6) in the Appendix. The components of the matrixes in (12), (13) and (14) can be found in the Appendix. By substituting the stress resultants from (11) into (5) and (6), the governing equations of the plate are obtained as

$$\begin{aligned} D_{66}^{kj} U_j'' + D_{26}^{kj} V_j'' + (B_{36}^{kj} - B_{45}^{jk}) W_j' - A_{55}^{kj} U_j - A_{45}^{kj} V_j &= A_{55}^k C_3 y \\ D_{26}^{kj} U_j'' + D_{22}^{kj} V_j'' + (B_{23}^{kj} - B_{44}^{jk}) W_j' - A_{45}^{kj} U_j - A_{44}^{kj} V_j &= A_{45}^k C_3 y \\ D_{44}^{kj} W_j'' + (B_{45}^{kj} - B_{36}^{jk}) U_j' + (B_{44}^{kj} - B_{23}^{jk}) V_j' - A_{33}^{kj} W_j &= \\ -(\tilde{A}_{36}^k + B_{45}^k) C_3 + \tilde{A}_{13}^k C_5 + A_{13}^k C_6 - B_{3T}^{jk} T_j - B_{3M}^{jk} M_j \end{aligned} \quad (15)$$

$$\begin{aligned} \int_{-b}^b (B_{16}^k U_k' + B_{12}^k V_k' + A_{13}^k W_k) dy + \\ 2b(\bar{A}_{11} C_6 + \bar{A}_{11} C_5 - \bar{A}_{16} C_3 - A_{1T}^k T_k - A_{1M}^k M_k) &= 0 \\ \int_{-b}^b (\tilde{B}_{16}^k U_k' + \tilde{B}_{12}^k V_k' + \tilde{A}_{13}^k W_k) dy + \\ 2b(\bar{\bar{A}}_{11} C_6 + \bar{\bar{A}}_{11} C_5 - \bar{\bar{A}}_{16} C_3 - \tilde{A}_{1T}^k T_k - \tilde{A}_{1M}^k M_k) &= 0 \\ \int_{-b}^b (-\tilde{B}_{66}^k U_k' - \tilde{B}_{26}^k V_k' + B_{45}^k W_k' + A_{55}^k U_k + A_{45}^k V_k - \tilde{A}_{36}^k W_k) dy \\ + 2b(-\bar{\bar{A}}_{16} C_6 - \bar{\bar{A}}_{16} C_5 + \bar{\bar{A}}_{66}^k + \frac{1}{3} b^2 \bar{A}_{55}^k) C_3 + \tilde{A}_{6T}^k T_k + \tilde{A}_{6M}^k M_k &= 0 \end{aligned} \quad (16)$$

where \bar{A}_{pq} , $\bar{\bar{A}}_{pq}$ and $\bar{\bar{\bar{A}}}_{pq}$ are defined in the Appendix. The set of $3N+6$ ordinary differential equations in (15) and (16) must be solved simultaneously to obtain the $3(N+1)$ unknown functions U_k , V_k and W_k and 3 unknown constants C_3 , C_5 and C_6 .

3. Solution procedure

For solution of (15), the matrix of variables $\{\xi\}$ and $\{\eta\}$ is defined as (17), and (15) is written in terms of $\{\xi\}$ and $\{\eta\}$.

$$\begin{aligned} \{\xi\} &= \{U \}'^T \quad \{V \}'^T \quad \{W \}'^T \\ \{\eta\} &= \{U \}^T \quad \{V \}^T \quad \{W \}'^T \end{aligned} \quad (17)$$

where for example $\{W\}$ is a column matrix defined as $\{W\}^T = \{W_1, W_2, \dots, W_{N+1}\}$. Employing $\{\xi\}$ and $\{\eta\}$, the governing equations in (15) can be written in the matrix form as

$$\begin{aligned} \{\xi\}' &= [A] \{\eta\} + \{F_{31}\} C_3 y \\ \{\eta\}' &= [B] \{\xi\} + \{\bar{F}_T\} \{T\} + \{\bar{F}_M\} \{M\} \\ &+ \{F_{32}\} C_3 + \{F_5\} C_5 + \{F_6\} C_6 \end{aligned} \quad (18)$$

where the coefficient matrixes in (18) are defined in the Appendix and for instance the matrix of temperature change and moisture content change are defined as $\{T\}^T = \{T_1, T_2,$

$\dots, T_{N+1}\}$ and $\{M\}^T = \{M_1, M_2, \dots, M_{N+1}\}$. By differentiating the first equation in (18), and substituting from the second equation in (18) into it, $\{\eta\}$ is eliminated and the following second order equation is obtained

$$\begin{aligned} \{\xi\}'' &= [C] \{\xi\} + [A] \{F_T\} \{T\} + [A] \{F_M\} \{M\} + \\ &(\{F_{31}\} + [A] \{F_{32}\}) C_3 + [A] \{F_5\} C_5 + [A] \{F_6\} C_6 \end{aligned} \quad (19)$$

where $(C) = (A)(B)$. To solve (19), the eigen-values and eigen-vectors of (C) are obtained as

$$\begin{aligned} [C][U] &= [U][\Lambda^2] \\ [\Lambda^2] &= \text{diag}(\lambda_1^2, \lambda_2^2, \dots, \lambda_{3(N+1)}^2) \end{aligned} \quad (20)$$

(U) and (Λ^2) are $(N+1) \times (N+1)$ matrixes. Using (U) and (Λ^2) , equations (19) are decoupled and an analytical solution is obtained for $\{\xi\}$ as

$$\begin{aligned} \{\xi\} &= [U][Cosh(\lambda x)] \{K_1\} + [U][Sinh(\lambda x)] \{K_2\} \\ &- [C]^{-1} (\{F_{31}\} + [A] \{F_{32}\}) C_3 \\ &- [B]^{-1} (\{F_T\} \{T\} + \{F_M\} \{M\} + \{F_5\} C_5 + \{F_6\} C_6) \end{aligned} \quad (21)$$

in which $(Cosh(\lambda x))$ and $(Sinh(\lambda x))$ are diagonal matrices and are defined as

$$\begin{aligned} [Cosh(\lambda x)] &= \\ \text{diag}(Cosh(\lambda_1 x), Cosh(\lambda_2 x), \dots, Cosh(\lambda_{3(N+1)} x)) \\ [Sinh(\lambda x)] &= \\ \text{diag}(Sinh(\lambda_1 x), Sinh(\lambda_2 x), \dots, Sinh(\lambda_{3(N+1)} x)) \end{aligned} \quad (22)$$

and $\{K_1\}$ and $\{K_2\}$ are column matrices which each of them has $3N+3$ unknown integration constants. By substituting $\{\xi\}$ from (21) into the second equation in (18) and integrating with respect to y , $\{\eta\}$ is obtained as

$$\begin{aligned} \{\eta\} &= [B][U][\Lambda]^{-1} [Sinh(\lambda x)] \{K_1\} + \\ [B][U][\Lambda]^{-1} [Cosh(\lambda x)] \{K_2\} - [A]^{-1} \{F_{31}\} C_3 y \end{aligned} \quad (23)$$

and the equations in (16) are written in terms of $\{\xi\}$ and $\{\eta\}$ as

$$\begin{aligned} \int_{-b}^b \{M_1\} \{\xi\} dy + 2b\bar{A}_{11} C_6 + 2b\bar{\bar{A}}_{11} C_5 - 2b\bar{\bar{\bar{A}}}_{16} C_3 \\ - 2bA_{1T}^k T_k - 2bA_{1M}^k M_k = 0 \\ \int_{-b}^b \{M_2\} \{\xi\} dy + 2b\bar{\bar{A}}_{11} C_6 + 2b\bar{\bar{\bar{A}}}_{11} C_5 - 2b\bar{\bar{\bar{A}}}_{16} C_3 \\ - 2b\tilde{A}_{1T}^k T_k - 2b\tilde{A}_{1M}^k M_k = 0 \\ \int_{-b}^b (\{M_{31}\} \{\xi\} + \{M_{32}\} \{\eta\}) dy - 2b\bar{\bar{\bar{A}}}_{16} C_6 - 2b\bar{\bar{\bar{A}}}_{16} C_5 \\ + (2b\bar{\bar{\bar{A}}}_{66}^k + \frac{2}{3} b^3 \bar{A}_{55}^k) C_3 + 2b\tilde{A}_{6T}^k T_k + 2b\tilde{A}_{6M}^k M_k = 0 \end{aligned} \quad (24)$$

where the coefficient matrixes in (24) are defined as

$$\begin{aligned} \{M_1\} &= \{\{B_{16}\}^T \quad \{B_{12}\}^T \quad \{A_{13}\}^T\} \\ \{M_2\} &= \{\{\tilde{B}_{16}\}^T \quad \{\tilde{B}_{12}\}^T \quad \{\tilde{A}_{13}\}^T\} \\ \{M_{31}\} &= \{-\{\tilde{B}_{66}\}^T \quad -\{\tilde{B}_{26}\}^T \quad -\{\tilde{A}_{36}\}^T\} \\ \{M_{32}\} &= \{\{A_{55}\}^T \quad \{A_{45}\}^T \quad \{B_{45}\}^T\} \end{aligned} \quad (25)$$

and the free edges conditions of the plate at $y=\pm b$ in (8) can be written in the matrix form in terms of $\{\xi\}$ and $\{\eta\}$ as

$$\begin{aligned}
 & [P_1]\{\xi(\pm b)\} - [D_{2T}]\{T\} - [D_{2M}]\{M\} \\
 & + \{B_{12}\}C_6 + \{\tilde{B}_{12}\}C_5 - \{\tilde{B}_{26}\}C_3 = 0 \\
 & [P_2]\{\eta(\pm b)\} + \{B_{45}\}C_3(\pm b) = 0 \\
 & [P_3]\{\xi(\pm b)\} - [D_{6T}]\{T\} - [D_{6M}]\{M\} \\
 & + \{B_{16}\}C_6 + \{\tilde{B}_{16}\}C_5 - \{\tilde{B}_{66}\}C_3 = 0
 \end{aligned} \tag{26}$$

where (P_1) , (P_2) and (P_3) are defined as

$$\begin{aligned}
 [P_1] &= \{[D_{26}] \ [D_{22}] \ [B_{23}]\} \\
 [P_2] &= \{[B_{45}] \ [B_{44}] \ [D_{44}]\} \\
 [P_3] &= \{[D_{66}] \ [D_{26}] \ [B_{36}]\}
 \end{aligned} \tag{27}$$

Substituting (21) and (23) into (26) and (24) give a set of $6(N+1)+3$ linear algebraic equation which are solved simultaneously to obtained $6(N+1)+3$ unknown constants include $\{K_1\}$, $\{K_2\}$, C_3 , C_5 and C_6 .

4. Out of plane stresses

The out of plane stresses can be obtained by integrating the equilibrium equation. For example, the out of plane shear stress σ_{yz} at the n^{th} numerical surface i.e., $z=z_n$ can be obtained by integrating the equilibrium equation in y direction as

$$\begin{aligned}
 \sigma_{yz}(z = z_n) &= - \int_{z_1}^{z_n} \left(\frac{\partial \sigma_y}{\partial y} \right) dz = \\
 & - \int_{z_1}^{z_n} (C_{22}\Phi_k V_k'' + C_{23}\Phi_k' W_k' + C_{26}\Phi_k U_k'') dz
 \end{aligned} \tag{28}$$

by employing the definitions in (13), the above equation can be written as

$$\sigma_{yz}(z = z_n) = - \sum_{k=1}^n (B_{22}^k V_k'' + A_{23}^k W_k' + B_{26}^k U_k'') \tag{29}$$

σ_{xz} and σ_z can be obtained with the same procedure as

$$\begin{aligned}
 \sigma_{xz}(z = z_n) &= - \int_{z_1}^{z_n} \left(\frac{\partial \sigma_{xy}}{\partial y} \right) dz = \\
 & - \sum_{k=1}^n (B_{26}^k V_k'' + A_{36}^k W_k' + B_{66}^k U_k'')
 \end{aligned} \tag{30}$$

$$\begin{aligned}
 \sigma_z(z = z_n) &= - \int_{z_1}^{z_n} \left(\frac{\partial \sigma_{yz}}{\partial y} \right) dz = \\
 & - \sum_{k=1}^n (A_{44}^k V_k' + B_{44}^k W_k'' + A_{45}^k U_k') + \bar{A}_{45} C_3
 \end{aligned} \tag{31}$$

where \bar{A}_{45} in (31) is defined as

$$\bar{A}_{45} = \sum_{i=1}^n C_{45}^{(i)} t_i \tag{32}$$

On the other hand, the constitutive law can be used to obtain the stresses in the plies of the sandwich plate through the strain components. Because the out of plane strains are discontinuous at the numerical surfaces, the continuity of the out of plane stresses are not warranted at the interface of layers. Integrating the equilibrium equations to obtain the out of plane stresses increases the accuracy of the results.

Table 1 Mechanical properties of lamina and core (Brischetto 2013)

Material	E_1 GPa	$E_2=E_3$ GPa	$G_{12}=G_{13}$ GPa	G_{23} GPa	$\nu_{12}=\nu_{13}$	ν_{23}
Lamina	138	8.5	4.5	3.2	0.29	0.36
Core	3	3	1.071	1.071	0.4	0.4

Table 2 Hygrothermal properties of lamina and core (Brischetto 2013)

Material	α_1 1/K	$\alpha_2=\alpha_3$ 1/K	β_1	$\beta_2=\beta_3$
Lamina	-0.5×10^{-6}	43×10^{-6}	0	0.4×10^{-2}
Core	50×10^{-6}	50×10^{-6}	0.28×10^{-2}	0.28×10^{-2}

Table 3 Thermal conductivity and moisture diffusion coefficients of lamina and face (Brischetto 2013)

Material	k_{11} W/mK	$k_{22}=k_{33}$ W/mK	D_{11} m^2/s	$D_{22}=D_{33}$ m^2/s	D_{11} kg/ms	$D_{22}=D_{33}$ kg/ms
Lamina	4.2	0.7	4.4×10^{-3}	3.1×10^{-3}	7.04	4.96
Core	0.18	0.18	6.66×10^{-11}	6.66×10^{-11}	9.324×10^{-8}	9.324×10^{-8}

5. Numerical results and discussions

The core of the sandwich plate is made of flexible foam and the faces are laminated composite. The mechanical, thermal and hygroscopic properties of the lamina and core are presented in Tables 1 to 3. The thickness of the core is h_c and the thickness of the face is h_f and the total thickness of sandwich plate is $h=h_c+2h_f$. The width of the plate is $2b$ and the edges of the plate at $y=\pm b$ and $x=\pm L$ are free. The plate is imposed to thermal and hygroscopic loading conditions.

5.1 Investigation the accuracy of results

The accuracy of present solution is validated with predictions of the finite element method (FEM). A sandwich plate with cross-ply faces as $(0^\circ/90^\circ/\text{core}/90^\circ/0^\circ)$ is subjected to a uniform temperature change as $\Delta T=1^\circ\text{C}$. The thickness of the core is $h_c=0.4h$, the thickness of face is $h_f=0.3h$, and the plate width is considered as $2b=3h$. A three-dimensional finite element model is made in the commercial finite element code Ansys using solid46 element for analysis of the plate. The thickness of the faces

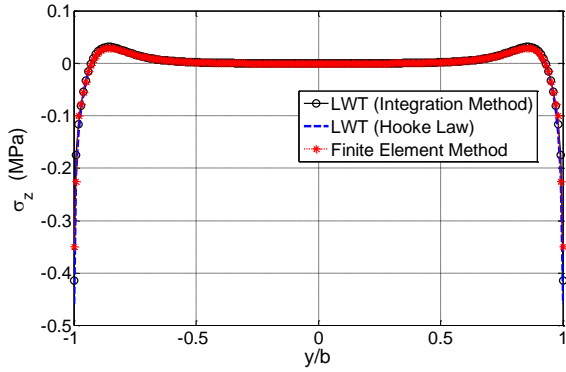


Fig. 2 Predictions of LWT and FEM for interlaminar thermal stress σ_z at core/face interface, $z=(h_c+h_f)/2$, of $(0^\circ/90^\circ/\text{core}/90^\circ/0^\circ)$ sandwich plate, ($\Delta T=1^\circ\text{C}$)

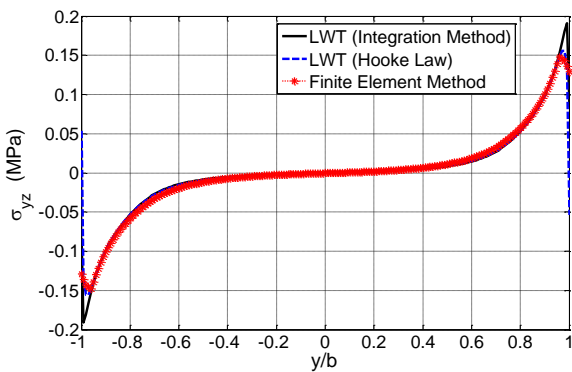


Fig. 3 Predictions of LWT and FEM for interlaminar shear stress σ_{yz} at $z=(h_c+h_f)/2$ of $(0^\circ/90^\circ/\text{core}/90^\circ/0^\circ)$ sandwich plate, ($\Delta T=1^\circ\text{C}$)

and the thickness of core are divided into 20 elements, the width of the plate is divided into 100 elements and the length are divided into 8 elements, and the uniform temperature change as $\Delta T=1^\circ\text{C}$ is imposed to the nodes.

Because of the mismatch between the coefficient of thermal expansion (CTE) of core, 0° layers and 90° layers in the faces, the thermal stresses arise in the laminate when the temperature of the plate changes. For example, CTE of lamina in the transverse direction is bigger than its CTE in the axial (fiber) direction. When the temperature of $(0^\circ/90^\circ/\text{core}/90^\circ/0^\circ)$ plate increases as ΔT , 0° layer in the face wants to expand in the y direction more than 90° layer, so shear stress σ_{yz} arises at the interfaces of $90^\circ/0^\circ$ interface in which, the direction of shear stress σ_{yz} at the interface on the 90° layers is from the center of plate toward the edge, and the direction of σ_{yz} on the 0° layers is from the edge toward the plate center. The out of plane stresses arise in vicinity of free edges especially near the interface of the layers with different thermo-mechanical properties. The predictions of LWT and FEM for out of plane normal stress σ_z along the width of the plate at $z=(h_c+h_f)/2$ is presented in Fig. 2. Except exactly at the free edge $y=b$, very good agreement is seen between the predictions of LWT and FEM for distribution of σ_z along the interface of layers. Exactly at the free edge, the prediction of LWT by Hooke's law is $\sigma_z=-0.4599$ MPa, the prediction of LW theory by the

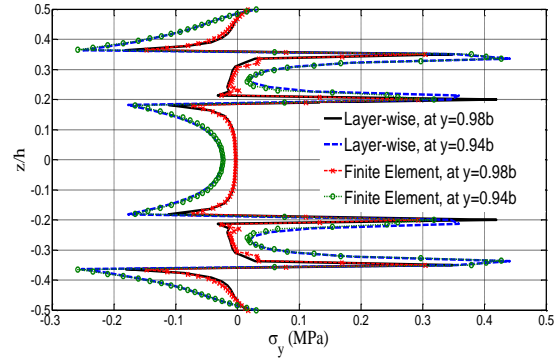


Fig. 4 Prediction of LWT and FEM for distribution of σ_y through the thickness of $(0^\circ/90^\circ/\text{core}/90^\circ/0^\circ)$ plate near the free edge, ($\Delta T=1^\circ\text{C}$)

Table 4 Global response of symmetric and un-symmetric cross-ply sandwich plate to uniform temperature change $\Delta T=1^\circ\text{C}$ ($h_f=0.3$, $h_c=0.4$, $2b=3h$)

Lamination	$C_6 \times 10^6$	$C_5 \times 10^6$ (1/mm)
$(90^\circ/90^\circ/\text{core}/90^\circ/90^\circ)$	4.4473	1.11×10^{-5}
$(90^\circ/90^\circ/\text{core}/0^\circ/0^\circ)$	21.4510	-59.0644
$(0^\circ/90^\circ/\text{core}/0^\circ/90^\circ)$	4.6250	3.7737
$(0^\circ/0^\circ/\text{core}/0^\circ/0^\circ)$	0.2545	-6.27×10^{-6}
$(90^\circ/90^\circ/\text{core}/90^\circ/90^\circ)$	48.0628	-1.878×10^{-6}

Table 5 Effect of layer stacking on the global response of plates to thermal loading ($\Delta T=1^\circ\text{C}$, $h_f=0.3$, $h_c=0.4$, $2b=3h$)

Lamination	$C_6 \times 10^6$	$C_5 \times 10^6$ (1/mm)	$C_3 \times 10^6$ (1/mm)
$(45^\circ/-45^\circ/\text{core}/-45^\circ/45^\circ)$	6.4587	8.9202×10^{-6}	-1.0040×10^{-5}
$(45^\circ/-45^\circ/\text{core}/45^\circ/-45^\circ)$	6.9311	2.4043×10^{-5}	-1.3028
$(45^\circ/45^\circ/\text{core}/-45^\circ/-45^\circ)$	22.7870	-6.4029×10^{-5}	-55.7552

integration method is $\sigma_z=-0.4141$ MPa and the prediction of FE method is -0.3501 MPa. Due to thermal load as $\Delta T=1^\circ\text{C}$, the plate expands at the axial direction, and the prediction of LWT and FEM for uniform axial strain of the plate is $C_6=4.4473 \times 10^{-6}$ and 4.4400×10^{-6} , respectively.

The predictions of LWT and FEM for out of plane shear stress σ_{yz} along the $90^\circ/0^\circ$ interface on the top face, $z=(h_c+h_f)/2$, are presented in Fig. 3. As it is seen in Fig. 3, at $90^\circ/0^\circ$ interface in the top face, the direction of σ_{yz} on 90° layer is positive for $y>0$ and is negative for $y<0$, which means that as expected the direction of shear stress σ_{yz} on 90° layer is from the plate center to the free edges. It is observed in Fig. 3 that near the free edges, prediction of LWT for σ_{yz} is bigger than the prediction of FEM. Fig. 4 shows the prediction of LWT and FEM for the in-plane normal stress σ_y through the thickness of the plate in the vicinity of the edge. In Fig. 4, good agreement is seen between the predictions of LWT and FEM for distribution of σ_y at the vicinity of free edge.

Comparison of the predictions of the LWT and FEM for out of plane and in-plane stresses shows that predictions of

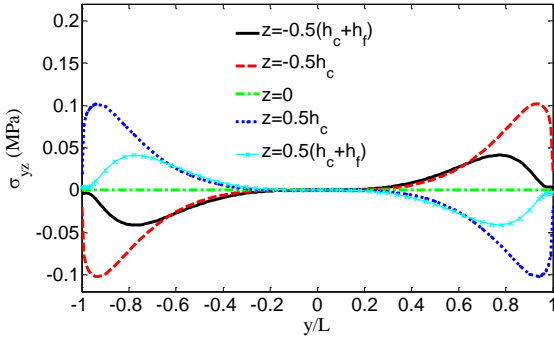


Fig. 5 Out of plane shear stress σ_{yz} along the width of symmetric (45°/-45°/core/-45°/45°) plate ($\Delta T=1^\circ\text{C}$)

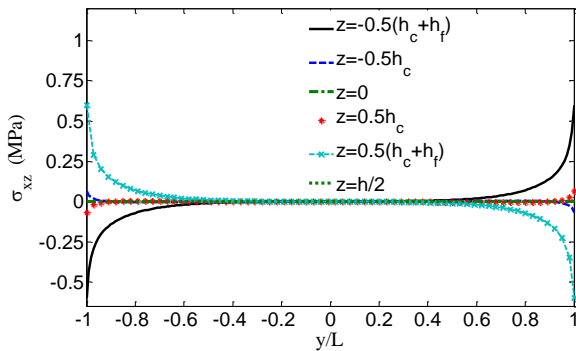


Fig. 6 Out of plane shear stress σ_{xz} along the width of symmetric (45°/-45°/core/-45°/45°) plate ($\Delta T=1^\circ\text{C}$)

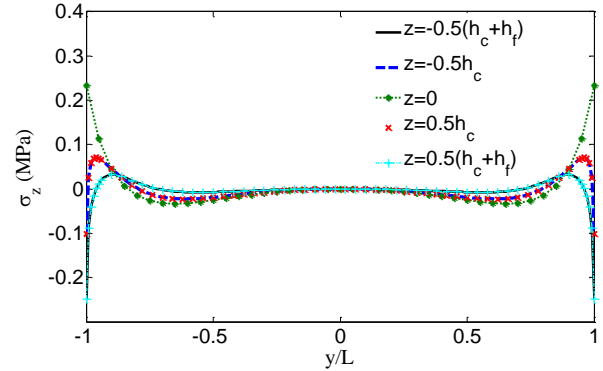


Fig. 7 Out of plane normal stress σ_z along the width of symmetric (45°/-45°/core/-45°/45°) plate ($\Delta T=1^\circ\text{C}$)

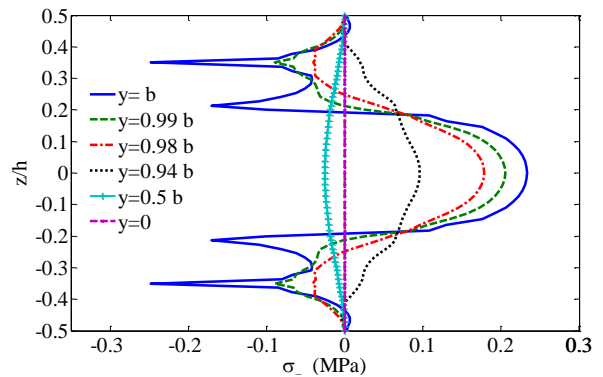


Fig. 8 Distribution of σ_z in symmetric (45°/-45°/core/-45°/45°) plate ($\Delta T=1^\circ\text{C}$)

LWT are in good agreement with predictions of FEM, except for interlaminar stresses σ_z and σ_{yz} exactly in the vicinity of free edges at the interface. Some researchers reported singularity of out of plane normal stresses in the interface of layers with different mechanical properties at the free edges.

5.2 Global deformation response

Due to the mismatch in the thermo-mechanical properties of the plies, even uniform temperature change in the plate may cause expansion, C_3 , bending C_5 , and twisting C_6 of the plate. C_6 is the uniform axial strain of the plate at the mid plane, C_5 is the curvature of the plate due to bending and C_3 is the rotation angle per unit length of the plate about x -axis due to twisting of the plate.

The deformation constants C_5 and C_6 for the plate with symmetric and un-symmetric cross-ply lamination which is subjected to $\Delta T=1^\circ\text{C}$ are shown in Table 4. It is observed in Table 4 that C_5 is vanished for symmetric laminations and is not vanished for un-symmetric laminations. It means that uniform temperature change causes bending of the sandwich plate with un-symmetric lamination. C_3 vanishes for the cross-ply laminations which are shown in Table 4.

For further study on the effect of layer staking on the deformation of the plate due to uniform temperature change, C_6 , C_5 and C_3 for symmetric (45°/-45°/core/-45°/45°) and un-symmetric (45°/-45°/core/45°/-45°) and (45°/45°/core/-45°/-45°) sandwich plate which is subjected

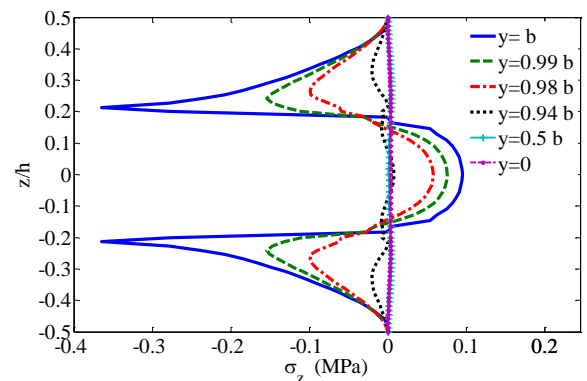


Fig. 9 Distribution of σ_z in un-symmetric (45°/45°/core/-45°/-45°) plate ($\Delta T=1^\circ\text{C}$)

to $\Delta T=1^\circ\text{C}$ are presented in Table 5. As seen in Table 5, C_5 and C_3 vanish in the symmetric (45°/-45°/core/-45°/45°) plate. It is seen that C_5 vanishes but C_3 does not vanish in the un-symmetric (45°/-45°/core/45°/-45°) and (45°/45°/core/-45°/-45°) plates.

5.3 Uniform thermal loading

Distribution of out of plane and in-plane stresses in the sandwich plate which is subjected to uniform temperature change is studied in this section. A symmetric (45°/-45°/core/-45°/45°) sandwich plate in which $h_f=0.3\text{ mm}$ and

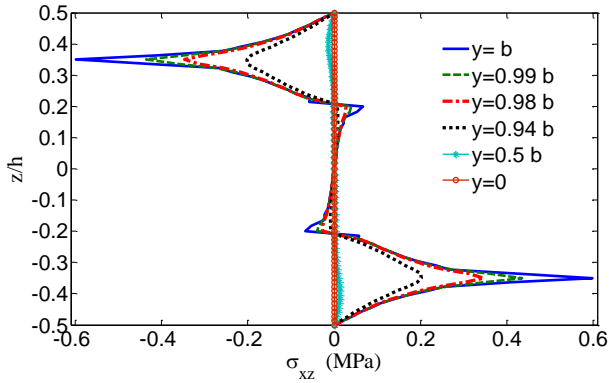


Fig. 10 Distribution of σ_{xz} in symmetric ($45^\circ/-45^\circ/\text{core}/-45^\circ/45^\circ$) plate ($\Delta T=1^\circ\text{C}$)

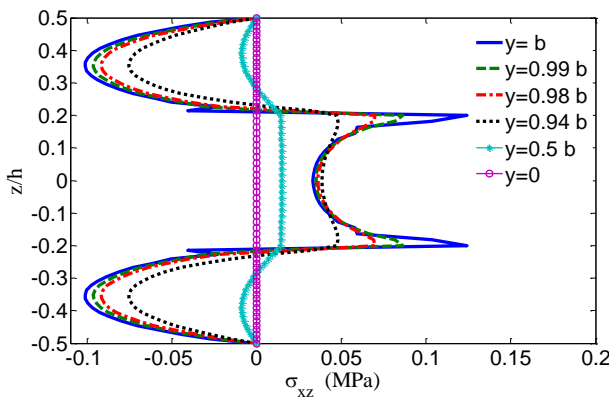


Fig. 11 Distribution of σ_{xz} in un-symmetric ($45^\circ/45^\circ/\text{core}/-45^\circ/-45^\circ$) plate ($\Delta T=1^\circ\text{C}$)

$h_m=0.4\text{ mm}$ is subjected to $\Delta T=1^\circ\text{C}$. The distribution of out of plane shear stresses σ_{yz} , σ_{xz} and normal stress σ_z at the interfaces along the width of the plate is shown in Figs. 5 to 7, respectively. The shear stresses σ_{yz} and σ_{xz} vanish at the mid plane of this plate at $z=0$. Also, the out of plane shear stresses vanishes at $y=0$, and asymmetric distribution is seen for the out of plane shear stresses with respect to z and y -coordinate. σ_z has symmetric distribution. In these figures, it is obvious that the out of plane stresses vanish far from the edges of the plate and arise near the edges. The shear stresses at $-45^\circ/45^\circ$ interfaces are bigger than the core/face interfaces. For $\Delta T=1^\circ\text{C}$, the maximum of σ_{yz} is about 0.105 MPa and the maximum of σ_{xz} is about 0.6MPa. The maximum of σ_z in compression is about -0.24MPa and its maximum in tension is 0.235MPa which are seen at $45^\circ/-45^\circ$ interface.

In order to study the distribution of stresses through the thickness and near the edge, the distribution of the stresses in the thickness of symmetric ($45^\circ/-45^\circ/\text{core}/-45^\circ/45^\circ$) and un-symmetric ($45^\circ/45^\circ/\text{core}/-45^\circ/-45^\circ$) plates is studied in the next figures.

The distribution of the normal stresses σ_z in these symmetric and un-symmetric plates is presented in Figs. 8 and 9, respectively. In the symmetric plate, the maximum of σ_z occurs at $-45^\circ/45^\circ$ interfaces and in the un-symmetric plate occurs near the core/face interface in the face. In both

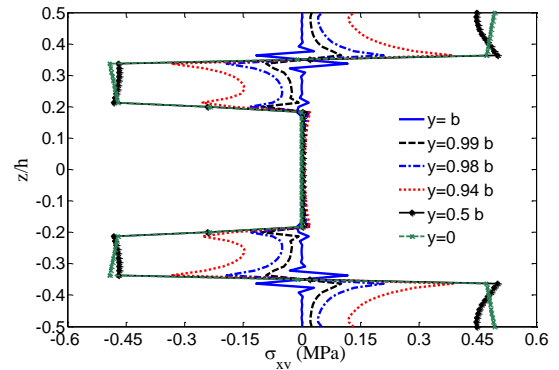


Fig. 12 Distribution of σ_{xy} in symmetric ($45^\circ/-45^\circ/\text{core}/-45^\circ/45^\circ$) plate ($\Delta T=1^\circ\text{C}$)

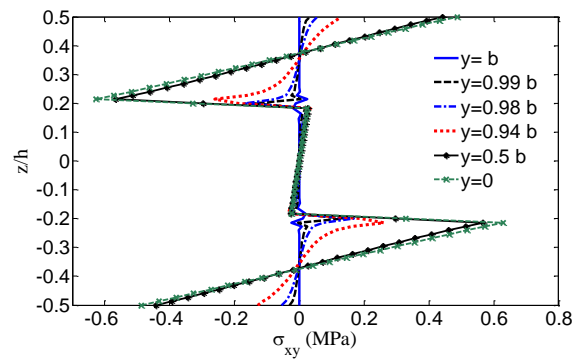


Fig. 13 Distribution of σ_{xy} in un-symmetric ($45^\circ/45^\circ/\text{core}/-45^\circ/-45^\circ$) plate ($\Delta T=1^\circ\text{C}$)

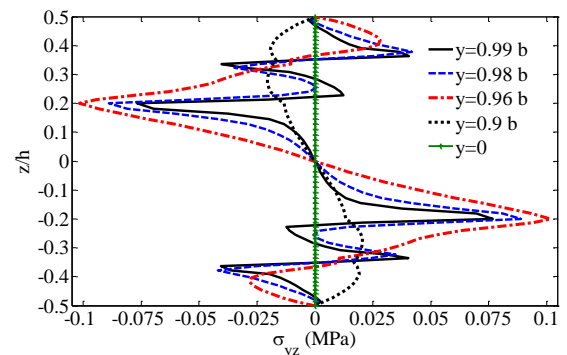


Fig. 14 Distribution of σ_{yz} in un-symmetric ($45^\circ/-45^\circ/\text{core}/-45^\circ/45^\circ$) plate, ($\Delta T=1^\circ\text{C}$)

plates, σ_z is positive in the core and is negative in the face and a sharp change is seen at the core/face interface. The positive normal stress σ_z at the core of symmetric plate is bigger than its maximum at the core of un-symmetric plate, and the compressive stress at the faces of un-symmetric plate is bigger than in the symmetric plate.

The distribution of the out of plane shear stress σ_{xz} in these symmetric an un-symmetric sandwich plate is shown in Figs. 10 and 11. In the symmetric plate, σ_{xz} is very small in the core and increases in the faces, and its maximum is at $-45^\circ/45^\circ$ interfaces. As seen in Figs. 10 and 11, the distribution of σ_{xz} in the un-symmetric plate is completely different from symmetric plate.

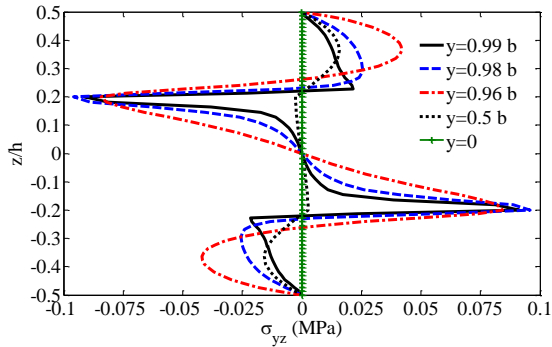


Fig. 15 Distribution of σ_{yz} in un-symmetric ($45^\circ/45^\circ/\text{core}/-45^\circ/-45^\circ$) plate, ($\Delta T=1^\circ\text{C}$)

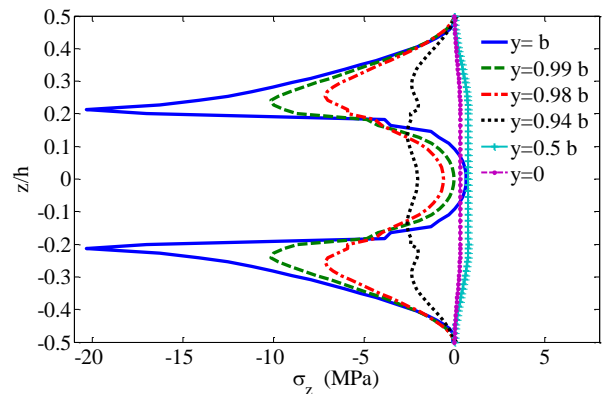


Fig. 18 Distribution of σ_z in un-symmetric ($45^\circ/45^\circ/\text{core}/-45^\circ/-45^\circ$) plate subjected to hygroscopic load ($\Delta M=1\%$)

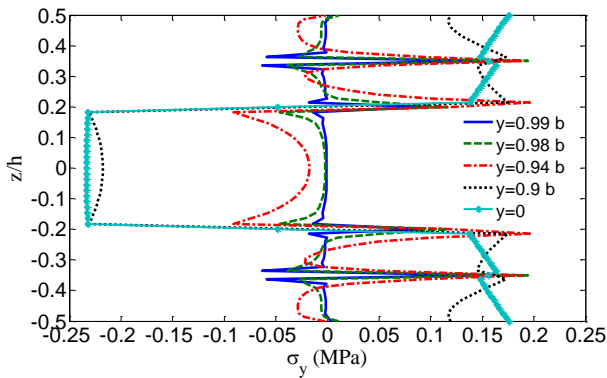


Fig. 16 Distribution of in-plane normal stress σ_y in un-symmetric ($45^\circ/45^\circ/\text{core}/-45^\circ/45^\circ$) plate, ($\Delta T=1^\circ\text{C}$)

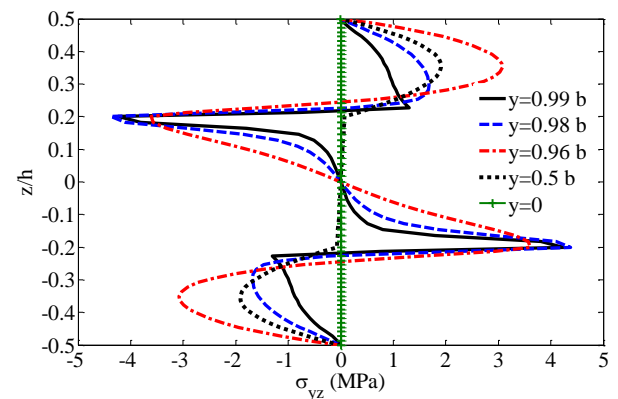


Fig. 19 Distribution of shear stress σ_{yz} in un-symmetric ($45^\circ/45^\circ/\text{core}/-45^\circ/-45^\circ$) plate subjected to hygroscopic load ($\Delta M=1\%$)

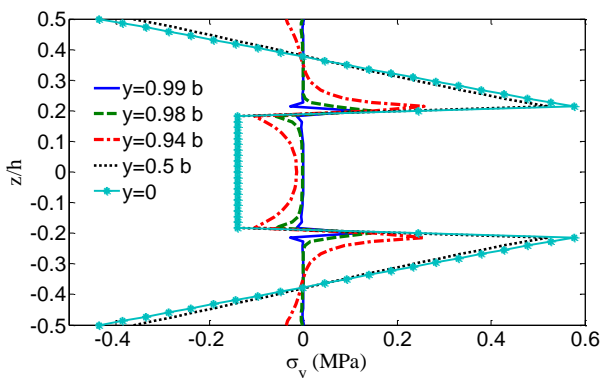


Fig. 17 Distribution of in-plane normal stress σ_y in un-symmetric ($45^\circ/45^\circ/\text{core}/-45^\circ/-45^\circ$) plate, ($\Delta T=1^\circ\text{C}$)

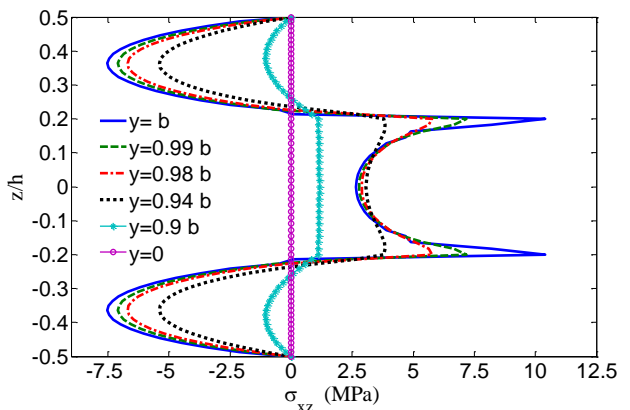


Fig. 20 Distribution of σ_{xz} in un-symmetric ($45^\circ/45^\circ/\text{core}/-45^\circ/-45^\circ$) plate subjected to hygroscopic load ($\Delta M=1\%$)

The distribution of the in-plane shear stress σ_{xy} through the thickness of ($45^\circ/-45^\circ/\text{core}/-45^\circ/45^\circ$) and ($45^\circ/45^\circ/\text{core}/-45^\circ/-45^\circ$) plate which is subjected to $\Delta T=1^\circ\text{C}$ is shown in Figs. 12 and 13, respectively. The in-plane shear stress σ_{xy} is discontinuous at $-45^\circ/45^\circ$ interfaces and at core/face interface and decreases by decreasing the distance to the free edge. σ_{xy} vanishes at free edges $y=\pm b$.

The distribution of the out of plane shear stress σ_{yz} in these symmetric and un-symmetric plates is presented in Figs. 14 and 15, respectively. The variation of σ_{yz} at the interfaces of physical layers is seen clearly in these figures.

The distribution of in-plane normal stress σ_y in these plates is presented in Figs. 16 and 17, respectively. As seen, σ_y decreases by decreasing the distance to the free edge.

5.4 Uniform hygroscopic loading

The sandwich plate which is subjected to uniform moisture content change is considered and the distribution

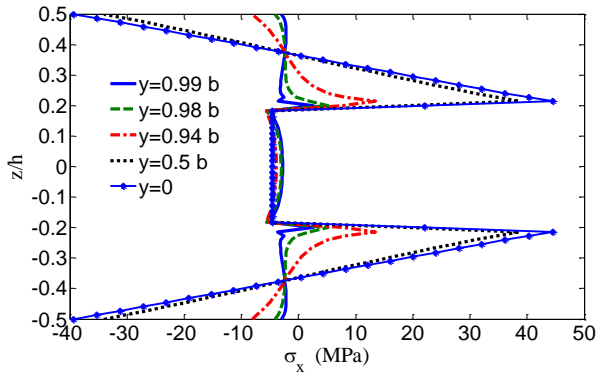


Fig. 21 Distribution of in-plane stress σ_x in un-symmetric ($45^\circ/45^\circ/\text{core}/-45^\circ/-45^\circ$) plate subjected to hygroscopic load ($\Delta M=1\%$)

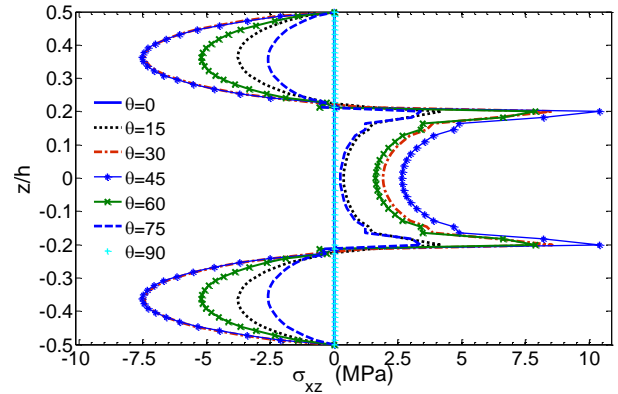


Fig. 24 Fiber directions effect on the distribution of σ_{xz} through the thickness of ($\theta/\theta/\text{core}/-\theta/-\theta$) plate ($\Delta M=1\%$)

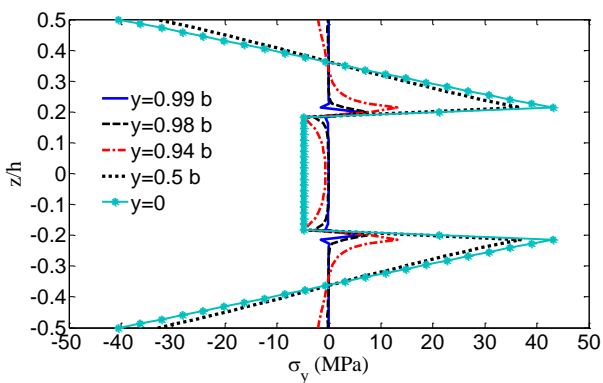


Fig. 22 Distribution of in-plane normal stress σ_y in un-symmetric ($45^\circ/45^\circ/\text{core}/-45^\circ/-45^\circ$) plate subjected to hygroscopic load ($\Delta M=1\%$)

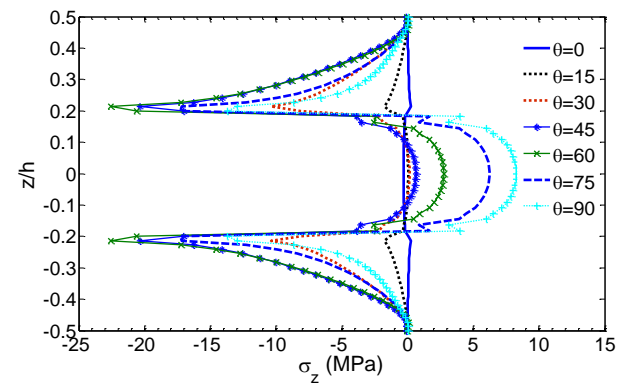


Fig. 25 Fiber directions effect on the distribution of σ_z through the thickness of ($\theta/\theta/\text{core}/-\theta/-\theta$) plate θ ($\Delta M=1\%$)

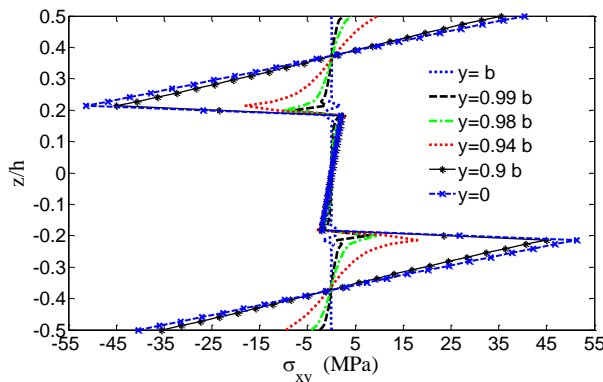


Fig. 23 Distribution of in-plane shear stress σ_{xy} in un-symmetric ($45^\circ/45^\circ/\text{core}/-45^\circ/-45^\circ$) plate subjected to hygroscopic load ($\Delta M=1\%$)

of in-plane and out of plane stresses is studied. The un-symmetric ($45^\circ/45^\circ/\text{core}/-45^\circ/-45^\circ$) sandwich plate layer is subjected to moisture content change as $\Delta M=1\%$. Distribution of the σ_z due to hygroscopic load $\Delta M=1\%$ is presented in Fig. 18. It is seen that σ_z is maximum (about -21MPa) at the free edge at the faces near the core/face interface. The distribution of σ_z is symmetric in the plate thickness. The distribution of the shear stresses σ_{yz} and σ_{xz}

through the thickness of the plate is depicted in Figs. 19 and 20. σ_{yz} increases sharply near the core/face interface near the edge and its maximum is about 4.5MPa . The hygroscopic shear stress σ_{yz} has asymmetric distribution through the thickness of the plate. It is observed in Fig. 20 that the maximum of σ_{xz} is about 10.4MPa at the core/face interface. The maximum value of σ_{xz} at the core/face interface is about 2.3 times greater than the σ_{yz} stress at the core/face interface.

The distribution of σ_x and σ_y and σ_{xy} in un-symmetric ($45^\circ/45^\circ/\text{core}/-45^\circ/-45^\circ$) plate are shown in Figs. 20 to 22, respectively. Because the edges of the plate are free at $y=\pm b$ and $x=\pm L$, as it is observed in Figs. 21 and 22, at $y=0$ and at $y=0.5b$ (far from the edges of plate), the distribution of σ_y is almost the same as distribution of σ_x at $y=0$ and at $y=0.5b$. The maximum of σ_x and σ_y is about -40MPa , and is observed at $y=0$, at the top and bottom surface of the plate, and is about 44MPa at the core/face interface. As seen in Fig. 23, σ_{xy} in the face changes almost linearly from -40MPa at the bottom surface of the plate to about 51MPa at the core/face interface.

In order to study the effect of plies stacking angles θ on the distribution of the stresses, σ_{xz} and σ_z at the free edge $y=b$ of ($\theta/\theta/\text{core}/-\theta/-\theta$) plate for various θ is presented in Figs. 24 and 25, respectively. It is seen that overlay the magnitude of σ_{xz} at the edge is maximum for $\theta=45^\circ$.

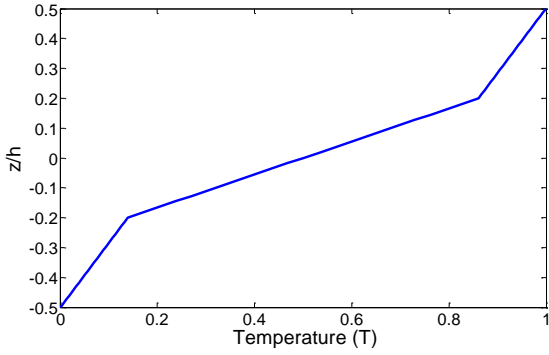


Fig. 26 Steady state temperature gradient in the thickness of the plate ($\Delta T_b=0^\circ\text{C}$, $\Delta T_i=1^\circ\text{C}$)

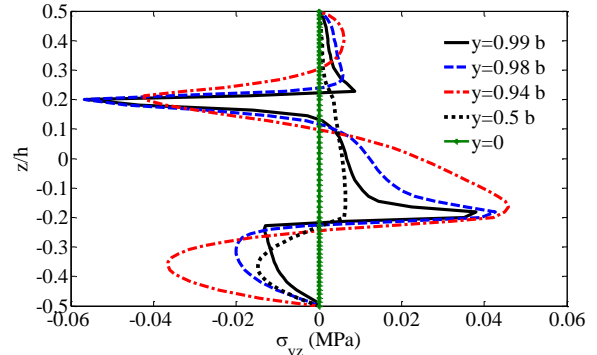


Fig. 30 Distribution of σ_{yz} in $(45^\circ/45^\circ/\text{core}/-45^\circ/-45^\circ)$ plate, non-uniform temperature change, $\Delta T_b=0^\circ\text{C}$ and $\Delta T_i=1^\circ\text{C}$

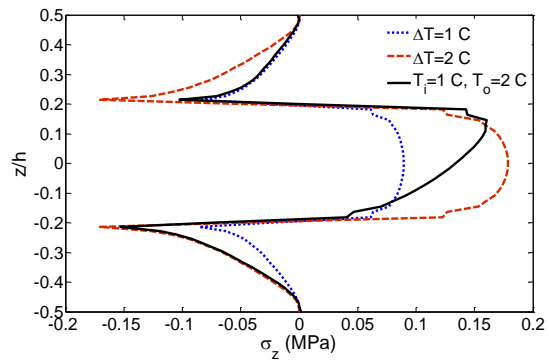


Fig. 27 Interlaminar normal stress at $y=b$ in $(0^\circ/0^\circ/\text{core}/0^\circ/0^\circ)$ plate, uniform and non-uniform temperature change

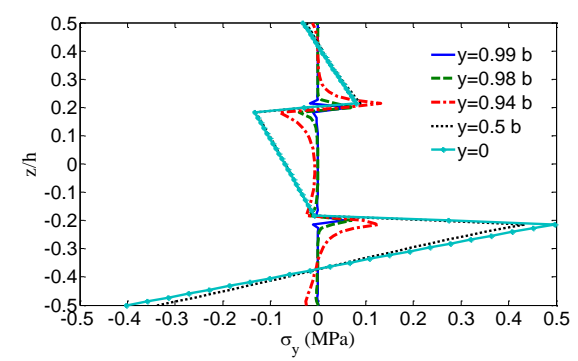


Fig. 31 Distribution of σ_y in $(45^\circ/45^\circ/\text{core}/-45^\circ/-45^\circ)$ plate, non-uniform temperature change, $\Delta T_b=0^\circ\text{C}$ and $\Delta T_i=1^\circ\text{C}$

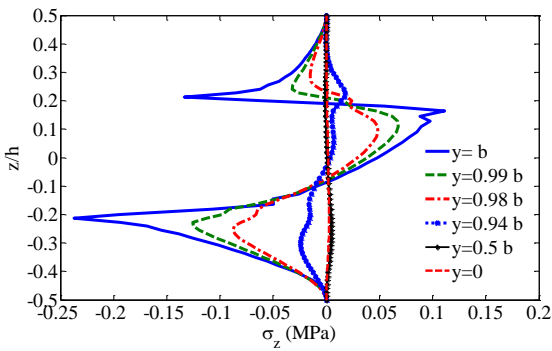


Fig. 28 Distribution of σ_z in $(45^\circ/45^\circ/\text{core}/-45^\circ/-45^\circ)$ plate, non-uniform temperature change, $\Delta T_b=0^\circ\text{C}$ and $\Delta T_i=1^\circ\text{C}$

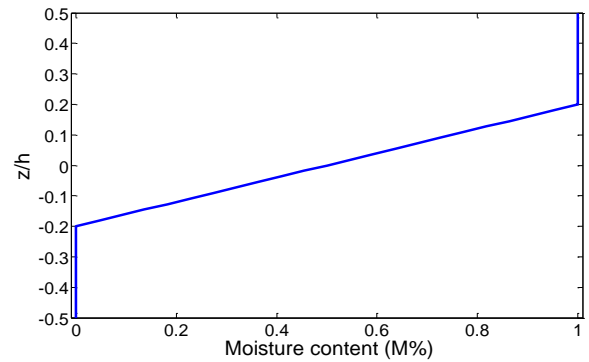


Fig. 32 Distribution of steady state moisture content in the thickness of the plate, $\Delta M_b=0\%$, $\Delta M_i=1\%$

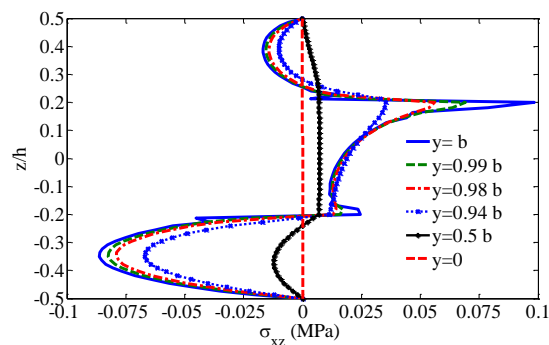


Fig. 29 Distribution of σ_{xz} in $(45^\circ/45^\circ/\text{core}/-45^\circ/-45^\circ)$ plate, non-uniform temperature change, $\Delta T_b=0^\circ\text{C}$ and $\Delta T_i=1^\circ\text{C}$

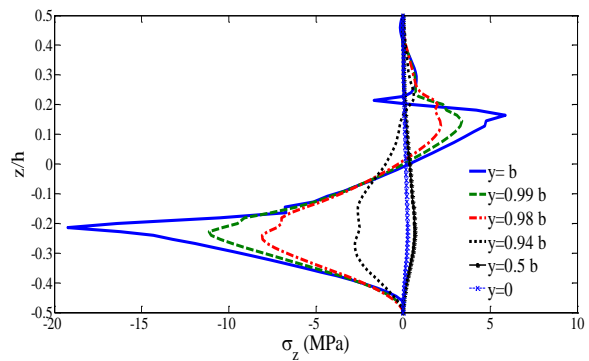


Fig. 33 Distribution of σ_z in $(45^\circ/45^\circ/\text{core}/-45^\circ/-45^\circ)$ plate, non-uniform moisture content change, $\Delta M_b=0\%$, $\Delta M_i=1\%$

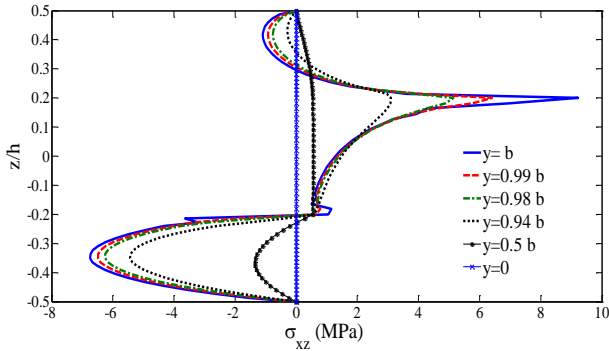


Fig. 34 Distribution of σ_{xz} in $(45^\circ/45^\circ/\text{core}/-45^\circ/-45^\circ)$ plate, non-uniform moisture content change, $\Delta M_b=0\%$, $\Delta M_t=1\%$

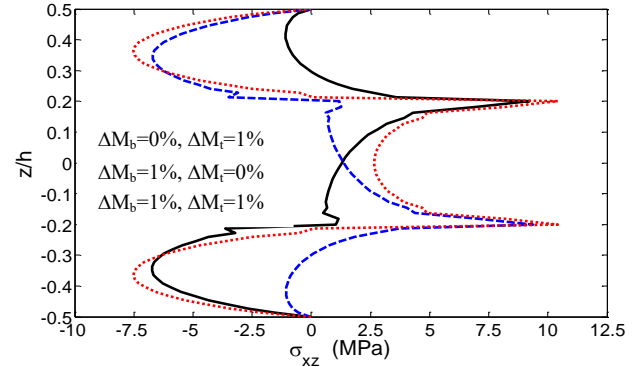


Fig. 37 Comparison of the distribution of σ_{xz} at $y=b$ in $(45^\circ/45^\circ/\text{core}/-45^\circ/-45^\circ)$ plate, uniform and non-uniform moisture content change

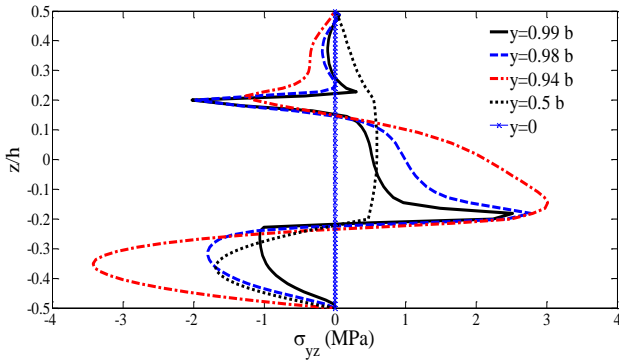


Fig. 35 Distribution of σ_{yz} in $(45^\circ/45^\circ/\text{core}/-45^\circ/-45^\circ)$ plate, non-uniform moisture content change, $\Delta M_b=0\%$, $\Delta M_t=1\%$

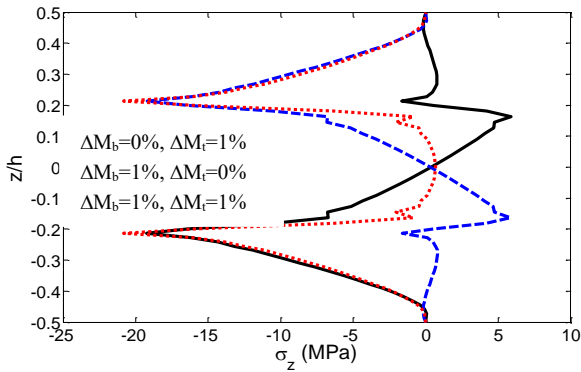


Fig. 36 Comparison of the distribution of σ_z at $y=b$ in $(45^\circ/45^\circ/\text{core}/-45^\circ/-45^\circ)$ plate, uniform and non-uniform moisture content change

5.5 Non-uniform hygrothermal loading

5.5.1 Temperature gradient in the thickness

The sandwich plate is subjected to steady state temperature gradient in the plate thickness, so that bottom surface of the plate is subjected to temperature change as ΔT_b and the top surface as ΔT_t , and temperature is uniform in the length and width of the plate. For temperature gradient in the 1D steady state heat transfer in the thickness of the sandwich plate which $\Delta T_b=0^\circ\text{C}$ and $\Delta T_t=1^\circ\text{C}$ is shown in Fig. 26. The thermal conductivities of the core and lamina are shown in Table 3. The distribution of σ_z at $y=b$

in $(0^\circ/0^\circ/\text{core}/0^\circ/0^\circ)$ plate for uniform temperature change and non-uniform temperature change are shown in Fig. 26. This figure compares the stresses in the plate for $\Delta T=1^\circ\text{C}$, $\Delta T=2^\circ\text{C}$ and for non-uniform temperature change as $\Delta T_b=1^\circ\text{C}$ and $\Delta T_t=2^\circ\text{C}$. The distribution of σ_z in the thickness of $(45^\circ/45^\circ/\text{core}/-45^\circ/-45^\circ)$ plate which is subjected to non-uniform temperature distribution $\Delta T_b=0^\circ\text{C}$ and $\Delta T_t=1^\circ\text{C}$ is shown in Fig. 28, and the distribution of σ_{xz} , σ_{yz} and σ_y are depicted in Figs. 29 to 31, respectively.

5.5.2 Moisture content gradient in the thickness

The stresses in the sandwich plate due to moisture content gradient are studied in next figures. The distribution of the steady state moisture content in the $(45^\circ/45^\circ/\text{core}/-45^\circ/-45^\circ)$ sandwich plate which the bottom surface is kept at $\Delta M_b=0$ and the top surface is kept at $\Delta M_t=1\%$ is shown in Fig. 32. The hygroscopic properties of the lamina and core are given in Table 3. As shown in Table 3, because D_{33} of the lamina is very bigger than of core, the distribution of the moisture contents is almost uniform in the top and bottom faces and linearly changed in the core. The distribution of hygroscopic stresses in $(45^\circ/45^\circ/\text{core}/-45^\circ/-45^\circ)$ plate for moisture content change as shown in Fig. 32 is shown in Figs. 33 to 35. To compare the hygrothermal stresses for uniform and non-uniform moisture change, the distribution of σ_z and σ_{xz} at $y=b$ in $(45^\circ/45^\circ/\text{core}/-45^\circ/-45^\circ)$ plate which is subjected to uniform moisture content change as $\Delta M_b=\Delta M_t=1\%$, and non-uniform distribution $\Delta M_b=0\%$, $\Delta M_t=1\%$ and non-uniform distribution $\Delta M_b=1\%$, $\Delta M_t=0\%$ are shown in Figs. 36 and 37, respectively. These figures compare the stress distribution for 3 kind of moisture distribution through the thickness of the plate.

6. Conclusions

The 3D hygrothermal stresses and free edge effect in the sandwich plate for uniform and through the thickness gradient hygrothermal loading are studied. The principle of minimum total potential energy is employed to obtain the governing equations and the layerwise discretization approach is used to obtain the free edge stresses in the

sandwich plate subjected to hygrothermal loading. The governing equations of the plate are solved for free boundary conditions to obtain the three-dimensional stresses. The FE modeling is used to verify the results of the present solution. The stresses and deformation of the symmetric and un-symmetric sandwich plate due to uniform and steady state through the thickness temperature and moisture gradient is studied and the results are compared. Various numerical results are presented and the effects of stacking sequence, fiber directions on loading gradient on the stress distribution are investigated.

References

- Ahmadi I. (2016), "Edge stresses analysis in thick composite panels subjected to axial loading using layerwise formulation", *Struct. Eng. Mech.*, **57**(4), 733-762.
- Ahmadi I. and Aghdam, M.M. (2010), "A generalized plane strain meshless local Petrov-Galerkin method for the micromechanics of thermomechanical loading of composites", *J. Mech. Mater. Struct.*, **5**(4), 549-566.
- Ahmadi I. and Aghdam, M.M. (2010), "Analysis of micro-stresses in the SiC/Ti metal matrix composite using a truly local meshless method", *J. Mech. Eng. Sci.*, **224**(8), 1567-1577.
- Ahmadi, I. (2016), "Edge stresses analysis in laminated thick sandwich cylinder subjected to distributed hygrothermal loading", *J. Sandw. Struct. Mater.*, 1099636216657681.
- Ahmadi, I. (2017), "A Galerkin layerwise Formulation for three-dimensional stress analysis in long sandwich plates", *Steel Compos. Struct.*, **24**(5), 523-536.
- Ahmadi, I. and Najafi, M. (2016), Three-dimensional stresses analysis in rotating thin laminated composite cylindrical shells. *Steel Compos. Struct.*, **22**(5), 1193-1214.
- Benkhedda, A., Tounsi, A. and Adda Bedia, E.A. (2008), "Effect of temperature and humidity on transient hygrothermal stresses during moisture desorption in laminated composite plates", *Compos. Struct.*, **82**, 623-635.
- Boukert, B., Benkhedda, A., Bedia, E.A. and Khodjet-Kesba, M. (2017), "Hygrothermoelastic behavior of thick composite plates using high order theory", *Proc. Struct. Integr.*, **5**, 115-122.
- Brischetto, S. (2012), "Hygrothermal loading effects in bending analysis of multilayered composite plates", *CMES-Comput. Model. Eng. Sci.*, **88**(5), 367-418.
- Brischetto, S. (2013), "Hygrothermoelastic analysis of multilayered composite and sandwich shells", *J. Sandw. Struct. Mater.*, **15**(2), 168-202.
- Cho, M. and Kim, H.S. (2000), "Iterative free-edge stress analysis of composite laminates under extension, bending, twisting and thermal loadings", *J. Sol. Struct.*, **37**, 435-459.
- Davi, G. and Milazzo, A. (1997), "Boundary element solution for free edge stresses in composite laminates", *J. Appl. Mech.*, **64**(4), 877-884.
- Farley, G.L. and Herakovich, C.T. (1978), "Influence of two-dimensional hygrothermal gradients on interlaminar stresses near free edges", *Adv. Compos. Mater.-Environ. Effects*, 143-159.
- Goodsell, J., Pagano, N.J., Kravchenko, O. and Pipes, R.B. (2013), "Interlaminar stresses in composite laminates subjected to anticlastic bending deformation", *J. Appl. Mech.*, **80**(4), 041020.
- Goodsell, J. and Pipes, R.B. (2016), "Free-edge interlaminar stresses in angle-ply laminates: A family of analytic solutions", *J. Appl. Mech.*, **83**(5), 051010.
- Hayashi, T. (1967), "Analytical study of interlaminar shear stresses in a laminated composite plate", *Trans. Jap. Soc. Aeronaut. Eng. Space Sci.*, **10**(17), 43-48.
- Herakovich, C.T. (1976), "On thermal edge effects in composite laminates", *J. Mech. Sci.*, **18**(3), 129-134.
- Huang, B. and Kim, H.S. (2015), "Interlaminar stress analysis of piezo-bonded composite laminates using the extended Kantorovich method", *J. Mech. Sci.*, **90**, 16-24.
- Kant, T. and Swaminathan, K. (2000), "Estimation of transverse/interlaminar stresses in laminated composites-a selective review and survey of current developments", *Compos. Struct.*, **49**, 65-75.
- Kim, H.S., Cho, M., Lee, J., Deheeger, A., Grediac, M. and Mathias, J.D. (2010), "Three-dimensional stress analysis of a composite patch using stress functions", *J. Mech. Sci.*, **52**, 1646-1659.
- Kim, T. and Atluri, S.N. (1995), "Analysis of edge stresses in composite laminates under combined thermo-mechanical loading, using a complementary energy approach", *Comput. Mech.*, **16**, 83-97.
- Lee, S.S. and Kim, B.S. (1997), "Boundary element analysis of singular thermal stresses in a unidirectional laminate", *Struct. Eng. Mech.*, **5**(6), 705-713.
- Lekhnitskii, S.G. (1981), *Theory of Elasticity of an Anisotropic Body*, Mir Publisher, Moscow, 104.
- Lo, S.H., Zhen, W.U., Cheung, Y.K. and Wanji, C. (2010), "Hygrothermal effects on multilayered composite plates using a refined higher order theory", *Compos. Struct.*, **92**, 633-646.
- Lu, X. and Liu, D. (1992), "An interlaminar shear stress continuity theory for both thin and thick composite laminates", *J. Appl. Mech.*, **59**(3), 502-509.
- Matsunaga, H. (2004), "A comparison between 2-D single-layer and 3-D layerwise theories for computing interlaminar stresses of laminated composite and sandwich plates subjected to thermal loadings", *Compos. Struct.*, **64**(2), 161-177.
- Mittelstedt, C. and Becker, W. (2004), "Interlaminar stress concentrations in layered structures-part I: A selective literature survey on the free-edge effect since 1967", *J. Compos. Mater.*, **38**, 1037-1062.
- Morton, S.K. and Webber, J.P.H. (1993), "Interlaminar failure due to mechanical and thermal stresses at the free edges of laminated plates", *Compos. Sci. Technol.*, **47**(1), 1-13.
- Morton, S.K. and Webber, J.P.H. (1993), "An analytical solution for the thermal stresses at the free-edges of laminated plates", *Compos. Sci. Technol.*, **46**, 175-185.
- Murugesan, N. and Rajamohan, V. (2015), "Investigation on interlaminar shear stresses in laminated composite beam under thermal and mechanical loading", *Steel Compos. Struct.*, **18**(3), 583-601.
- Murugesan, N. and Rajamohan, V. (2016), "Interlaminar shear stresses in laminated composite plates under thermal and mechanical loading", *Mech. Adv. Mater. Struct.*, **23**(5), 554-564.
- Naidu, N.V.S. and Sinha, P.K. (2005), "Nonlinear finite element analysis of laminated composite shells in hygrothermal environments", *Compos. Struct.*, **69**, 387-395.
- Nath, J.K. and Kapuria, S. (2013), "Global-local and zigzag-local theories for direct transverse shear stress computation in piezolaminated plates under thermal loading", *J. Mech. Sci.*, **75**, 158-169.
- Nguyen, T.D. and Nguyen, D.H. (2007), "Interlaminar stresses and delamination of composite laminates under extension and bending", *Struct. Eng. Mech.*, **25**(6).
- Padhi, A. and Pandit, M.K. (2016), "Behaviour of sandwich laminates subjected to thermal loading using higher-order zigzag theory", *J. Sandw. Struct. Mater.*, **18**(2), 174-199.
- Pagano, N.J. (1974), "On the calculation of interlaminar normal

stress in composite laminate”, *J. Compos. Mater.*, **8**(1), 65-81.

Pantano, A. and Averill, R.C. (2000), “A 3D zig-zag sublaminated model for analysis of thermal stresses in laminated composite and sandwich plate”, *J. Sandw. Struct. Mater.*, **2**(3), 288-312.

Patel, B.P., Ganapathi, M. and Makhecha, D.P. (2002), “Hygrothermal effects on the structural behaviour of thick composite laminates using higher-order theory”, *Compos. Struct.*, **56**, 25-34.

Puppo, A.H. and Evensen, H.A. (1970), “Interlaminar Shear in laminated composites under generalized plane stress”, *J. Compos. Mater.*, **4**, 204-220.

Singh, S.K. and Chakrabarti, A. (2017), “Hygrothermal analysis of laminated composites using C⁰ FE model based on higher order zigzag theory”, *Steel Compos. Struct.*, **23**(1), 41-51.

Tahani, M. and Nosier, A. (2003), “Free edge stress analysis of general cross-ply composite laminates under extension and thermal loading”, *Compos. Struct.*, **60**, 91-103.

Vaddadi, P., Nakamura, T. and Singh R.P. (2003), “Transient hygrothermal stresses in fiber reinforced composites: A heterogeneous characterization approach”, *Compos. Part A: Appl. Sci. Manufact.*, **34**(8), 719-730.

Wang, Y.R. and Chou, T.W. (1989), “Three-dimensional transient interlaminar thermal stresses in angle-ply composites”, *J. Appl. Mech.*, **56**(3), 601-608.

Wang, A.S.D. and Crossman, F.W. (1977), “Edge effects on thermally induced stresses in composite laminates”, *J. Compos. Mater.*, **11**, 300-312.

Wang, S.S. and Choi, I. (1982), “Boundary-layer hygroscopic stresses in angle-ply composite laminates”, *AIAA J.*, **20**(11), 1592-1598.

Yin, W.L. (1994), “Simple solution of the free-edge stresses in composite laminates under thermal and mechanical loads”, *J. Compos. Mater.*, **28**(6), 573-386.

Zenkour, A.M. (2012), “Hygrothermal analysis of exponentially graded rectangular plates”, *J. Mech. Mater. Struct.*, **7**(7), 687-700.

Zenkour, A.M., Mashat, D.S. and Alghanmi, R.A. (2014), “Hygrothermal analysis of antisymmetric cross-ply laminates using a refined plate theory”, *J. Mech. Mater. Des.*, **10**(2), 213-226.

Zhu, S.Q., Chen, X. and Wang, X. (2007), “Response of dynamic interlaminar stresses in laminated plates under free vibration and thermal load”, *Struct. Eng. Mech.*, **25**(6), 753-765.

Appendix

The interpolation function which is used in (2) is the linear Lagrangian interpolation function and are defined as

$$\Phi_k(z) = \begin{cases} \frac{1}{t_{k-1}}(z - z_k), & z \leq z_{k-1} \\ \frac{1}{t_k}(z_{k+1} - z), & z_{k-1} \leq z \leq z_k \\ 0, & z \leq z_{k-1} \text{ or } z \geq z_{k+1} \end{cases} \quad (A1)$$

where z_k is the thickness coordinate of k^{th} numerical surface and $t_{k-1} = z_{k+1} - z_k$ is the thickness of k^{th} numerical layer. Also the matrixes A_{pq}^{kj} , B_{pq}^{kj} and D_{pq}^{kj} which are defined in (12) are $(N+1) \times (N+1)$ matrixes and can be obtained as

$$(A_{pq}^{kj}, B_{pq}^{kj}) = \begin{cases} -\frac{\bar{C}_{pq}^{(k-1)}}{h_{k-1}}, -\frac{\bar{C}_{pq}^{(k-1)}}{2}, & \text{if } j = k - 1 \\ \frac{\bar{C}_{pq}^{(k-1)}}{h_{k-1}} + \frac{\bar{C}_{pq}^{(k)}}{h_k}, \frac{\bar{C}_{pq}^{(k-1)}}{2} - \frac{\bar{C}_{pq}^{(k)}}{2}, & \text{if } j = k \\ -\frac{\bar{C}_{pq}^{(k)}}{h_k}, \frac{\bar{C}_{pq}^{(k)}}{2}, & \text{if } j = k + 1 \\ (0, 0) & \text{if } j < k - 1 \text{ or } j > k + 1 \end{cases} \quad (A2)$$

$$D_{pq}^{kj} = \begin{cases} \frac{h_{k-1} \bar{C}_{pq}^{(k-1)}}{6} & \text{if } j = k - 1 \\ \frac{h_{k-1} \bar{C}_{pq}^{(k-1)}}{3} + \frac{h_k \bar{C}_{pq}^{(k)}}{3}, & \text{if } j = k \\ \frac{h_{k-1} \bar{C}_{pq}^{(k)}}{6} & \text{if } j = k + 1 \\ 0 & \text{if } j < k - 1 \text{ or } j > k + 1 \end{cases} \quad (A3)$$

and A_{pq}^k , \tilde{A}_{pq}^k , \tilde{B}_{pq}^k are $(N+1)$ column matrix and are obtained as

$$A_{pq}^k = \begin{cases} -\bar{C}_{pq}^{(1)}, & \text{if } k = 1 \\ \bar{C}_{pq}^{(k-1)} - \bar{C}_{pq}^{(k)}, & \text{if } 1 < k < N + 1 \\ \bar{C}_{pq}^{(N)}, & \text{if } k = N + 1 \end{cases} \quad (A4)$$

$$\tilde{A}_{pq}^k = \begin{cases} -\bar{C}_{pq}^{(1)} \left(\frac{z_2 + z_1}{2} \right), & \text{if } k = 1 \\ \bar{C}_{pq}^{(k-1)} \left(\frac{z_k + z_{k-1}}{2} \right) - \bar{C}_{pq}^{(k)} \left(\frac{z_{k+1} + z_k}{2} \right), & \text{if } 1 < k < N + 1 \\ \bar{C}_{pq}^{(N)} \left(\frac{z_{N+1} + z_N}{2} \right), & \text{if } k = N + 1 \end{cases}$$

$$\tilde{B}_{pq}^k = \begin{cases} t_1 \frac{\bar{C}_{pq}^{(1)}}{2} & \text{if } k = 1 \\ t_{k-1} \frac{\bar{C}_{pq}^{(k-1)}}{2} + t_k \frac{\bar{C}_{pq}^{(k)}}{2} & \text{if } 1 < k < N + 1 \\ t_N \frac{\bar{C}_{pq}^{(N)}}{2} & \text{if } k = N + 1 \end{cases} \quad (A5)$$

The matrix $\{\lambda\}$ and $\{\mu\}$ are used in (14) are defined as

$$\begin{aligned} \{\mu\}^{(k)} &= [\bar{C}]^{(k)} \{\alpha\}^{(k)} \\ \{\lambda\}^{(k)} &= [\bar{C}]^{(k)} \{\beta\}^{(k)} \\ \{\alpha\} &= \{\alpha_x, \alpha_y, \alpha_z, 0, 0, \alpha_{xy}\}^T \\ \{\beta\} &= \{\beta_x, \beta_y, \beta_z, 0, 0, \beta_{xy}\}^T \end{aligned} \quad (A6)$$

And the thermal and hygroscopic effect matrix are defined in (14) are obtained as

$$(B_{pT}^{kj}, D_{pT}^{kj}) = \begin{cases} \frac{\mu_p^{(k-1)}}{2}, t_{k-1} \frac{\mu_p^{(k-1)}}{6} & \text{if } j = k - 1 \\ \frac{\mu_p^{(k-1)}}{2} - \frac{\mu_p^{(k)}}{2}, t_{k-1} \frac{\mu_p^{(k-1)}}{3} + t_k \frac{\mu_p^{(k)}}{3}, & \text{if } j = k \\ \frac{\mu_p^{(k)}}{2}, t_{k-1} \frac{\mu_p^{(k)}}{6} & \text{if } j = k + 1 \\ (0, 0) & \text{if } j < k - 1 \text{ or } j > k + 1 \end{cases} \quad (A7)$$

$$(B_{pM}^{kj}, D_{pM}^{kj}) = \begin{cases} \frac{\lambda_p^{(k-1)}}{2}, t_{k-1} \frac{\lambda_p^{(k-1)}}{6} & \text{if } j = k - 1 \\ \frac{\lambda_p^{(k-1)}}{2} - \frac{\lambda_p^{(k)}}{2}, t_{k-1} \frac{\lambda_p^{(k-1)}}{3} + t_k \frac{\lambda_p^{(k)}}{3}, & \text{if } j = k \\ \frac{\lambda_p^{(k)}}{2}, t_{k-1} \frac{\lambda_p^{(k)}}{6} & \text{if } j = k + 1 \\ (0, 0) & \text{if } j < k - 1 \text{ or } j > k + 1 \end{cases} \quad (A8)$$

and A_{pT}^k , \tilde{A}_{pT}^k , A_{pM}^k and \tilde{A}_{pM}^k can be obtained as

$$A_{pT}^k = \begin{cases} -\mu_p^{(1)}, & \text{if } k = 1 \\ \mu_p^{(k-1)} - \mu_p^{(k)}, & \text{if } 1 < k < N + 1 \\ \mu_p^{(N)}, & \text{if } k = N + 1 \end{cases} \quad (A9)$$

$$\tilde{A}_{pT}^k = \begin{cases} -\mu_p^{(1)} \left(\frac{z_2 + z_1}{2} \right), & \text{if } k = 1 \\ \mu_p^{(k-1)} \left(\frac{z_k + z_{k-1}}{2} \right) - \mu_p^{(k)} \left(\frac{z_{k+1} + z_k}{2} \right), & \text{if } 1 < k < N + 1 \\ \mu_p^{(N)} \left(\frac{z_{N+1} + z_N}{2} \right), & \text{if } k = N + 1 \end{cases}$$

$$A_{pM}^k = \begin{cases} -\lambda_p^{(1)}, & \text{if } k = 1 \\ \lambda_p^{(k-1)} - \lambda_p^{(k)} & \text{if } 1 < k < N + 1 \\ \lambda_p^{(N)}, \lambda_p^{(N)} \left(\frac{z_{N+1} + z_N}{2} \right), & \text{if } k = N + 1 \end{cases} \quad (A10)$$

$$\tilde{A}_{pM}^k = \begin{cases} -\lambda_p^{(1)} \left(\frac{z_2 + z_1}{2} \right), & \text{if } k = 1 \\ \lambda_p^{(k-1)} \left(\frac{z_k + z_{k-1}}{2} \right) - \lambda_p^{(k)} \left(\frac{z_{k+1} + z_k}{2} \right), & \text{if } 1 < k < N + 1 \\ \lambda_p^{(N)} \left(\frac{z_{N+1} + z_N}{2} \right), & \text{if } k = N + 1 \end{cases}$$

and \bar{A}_{pq} , $\bar{\bar{A}}_{pq}$ and $\bar{\bar{\bar{A}}}_{pq}$ which are used in (16) are defined as

$$(\bar{A}_{pq}, \bar{\bar{A}}_{pq}, \bar{\bar{\bar{A}}}_{pq}) = \int_{-h/2}^{h/2} \bar{C}_{pq}^{(k)}(1, z, z^2) dz \quad (A11)$$

The matrixes which is used in (18) are defined as following

$$\begin{aligned} [A] &= [\hat{D}]^{-1} [\hat{A}] \\ \{F_{31}\} &= [\hat{D}]^{-1} \begin{Bmatrix} \{A_{55}\} \\ \{A_{45}\} \\ \{0\} \end{Bmatrix} \end{aligned} \quad (A12)$$

where the matrices in (A11) are defined as

$$\begin{aligned} [\hat{D}] &= \begin{bmatrix} [D_{66}] & [D_{26}] & [0] \\ [D_{26}] & [D_{22}] & [0] \\ [0] & [0] & [I] \end{bmatrix}, \\ [\hat{A}] &= \begin{bmatrix} [a_{11}] & [a_{12}] & [a_{13}] \\ [a_{21}] & [a_{22}] & [a_{23}] \\ [0] & [0] & [I] \end{bmatrix} \end{aligned} \quad (A13)$$

$$[a_{11}] = [A_{55}], [a_{12}] = [A_{45}], [a_{13}] = [\tilde{B}_{45}]^T - [B_{36}],$$

$$[a_{21}] = [A_{45}], [a_{22}] = [A_{44}], [a_{23}] = [B_{44}]^T - [B_{23}]$$

and (0) and (I) are $(N+1) \times (N+1)$ zero and identity matrix and

$$\begin{aligned} [B] &= \begin{bmatrix} [I] & [0] & [0] \\ [0] & [I] & [0] \\ [b_{31}] & [b_{32}] & [b_{33}] \end{bmatrix} \\ [b_{31}] &= [D_{44}]^{-1} ([B_{36}]^T - [B_{45}]), \\ [b_{32}] &= [D_{44}]^{-1} ([B_{23}]^T - [B_{44}]), \\ [b_{33}] &= [D_{44}]^{-1} [A_{33}] \end{aligned} \quad (A14)$$

and other matrix in (18) are defined as

$$\begin{aligned} \{F_{32}\} &= \{0\}^T \{0\}^T - [D_{44}]^{-1} (\{\tilde{A}_{36}\} + \{B_{45}\})^T \}^T \\ \{F_5\} &= \{0\}^T \{0\}^T [D_{44}]^{-1} \{\tilde{A}_{13}\}^T \}^T \\ \{F_6\} &= \{0\}^T \{0\}^T [D_{44}]^{-1} \{A_{13}\}^T \}^T \\ \{F_T\} &= \{0\} \{0\} - [D_{44}]^{-1} [B_{3T}]^T \}^T \\ \{F_M\} &= \{0\} \{0\} - [D_{44}]^{-1} [B_{3M}]^T \}^T \end{aligned} \quad (A15)$$